2019

Engineering magnetic properties of nanoparticles for biomedical applications and magnetic thin film composite heterostructures for device applications.

Shivakumar Hunagund

Engineering magnetic properties of nanoparticles for biomedical applications and magnetic thin film composite heterostructures for device applications.

A thesis submitted in partial fulfillment of the requirements for the Degree of Master of Science at Virginia Commonwealth University

by

Shivakumar Hunagund

Advisor: **Dr. Ravi Hadimani**

Assistant Professor

Department of Mechanical and Nuclear Engineering

Virginia Commonwealth University

Richmond Virginia

May 2019

Dedication

This dissertation is gratefully dedicated to my parents, sisters, beloved grandparents, and all of my friends, without whom none of my success would be possible.

Candidate's Certificate

I hereby declare that the work presented in this dissertation is original and was performed by me in the laboratory of Biomagnetism under the supervision of Dr. Ravi L. Hadimani, Assistant Professor in the Department of Mechanical and Nuclear Engineering, Virginia Commonwealth University, Richmond, Virginia. This dissertation work has not been submitted for a degree to any other University or Institution.

_____

Shivakumar G. Hunagund

Acknowledgements

Firstly, I would like to thank all the people who have helped me and gave moral support in working on my research project. I would like to thank my supervisor Dr. Ravi Hadimani for providing me such an opportunity to conduct research under his guidance. I would also like to thank the financial and technical support given to me by the Department of Mechanical and Nuclear Engineering. A very special thanks to Dr. Karla Mossi. I would like to gratefully acknowledge Dr. Ahmed El-Gendy from University of Texas El-Paso, for all his assistance and advice during my first year of study here at the VCU and also Prof. Vitalij Pecharsky and Dr. Shalabh Gupta for providing us with the nanomaterials to conduct research of Gadolinium Silicide nanomaterial for biomedical applications. In addition, I would like to thank my committee members, Dr. Karla Mossi and Dr. Dmitry Pestov for happily agreeing to serve in my committee and sharing their valuable thoughts about my research. I wish to thank my lab mate Shane Harstad for his help and support in my work. I would like to extend my support to Dr. Carlos Castano Londono from the Nanomaterials Core Characterization facility for depositing magnetic thin films and Dr. Gary Atkinson from the Virginia Microelectronics Center, VCU for helping me in getting trained on equipment at Clean room. Lastly, I would like to thank again my parents for believing in me and giving me the freedom to pursue my interests.

Table of contents

List of figures

Fig. 14 SEM image of the specimen S5. Note contrast visible at the interface between the Pt layer on top and the silicon substrate. Gd_5Si_4 is deposited on Fe_3O_4.

Fig. 15 AFM images of the Fe_3O_4 thin film shows surface roughness of 7.38 nm. The surface roughness was analyzed with Nanoscope analysis software.

Fig. 16 AFM images (Height, Phase and 3D) of the Fe_3O_4 - Gd_5Si_4 thin film. Analysis shows surface roughness of 3.02 nm.

Fig. 16 XPS Survey spectrum of Fe_3O_4 film indicating presence of carbon. Analysis reveals presence of phases other than Fe_3O_4. (right) Fe_3O_4 (XPS SPECTRUM) - Region: Fe2p3 spectrum curve fitted to identify peaks.

Fig. 17 XPS Survey spectrum of Fe_3O_4 film indicating presence of carbon. Analysis reveals presence of phases other than Fe_3O_4. (right) Fe_3O_4 (XPS SPECTRUM) - Region: Fe2p3 spectrum curve fitted to identify peaks.

Fig. 18 XPS SPECTRUM - Region: Gd4d/3 spectrum curve fitted to identify peaks. (bottom) Region: O1s/3 spectrum curve fitted to identify peaks.

Fig. 19 XPS SPECTRUM - Region: Si2p/3 spectrum curve fitted to identify peaks.

Fig. 20 Fe_3O_4 (S1) thin film exhibit ferromagnetic behavior with magnetic saturation at around 8 emu. The diamagnetic features in observed is due to glass/silicon substrate. (right) M-T Curve shows shift in moment by 0.60 emu at the temperature of 280K indicating possible transition.

Fig. 21 M-H curve of the Fe_3O_4 (S2) thin film showing magnetic saturation (Ms) at about 2.6 emu and Tc at 378 K.

Fig. 23 M-H curve of the Gd_5Si_4 - Fe_3O_4 (S4) bilayer thin film heterostructure retains ferromagnetic behavior. The magnetic saturation (Ms) is about 1.58 emu. Transition temperatures are observed at around 148 K, 240 K and 300 K. Note Gd_5Si_4 has Tc = 318 K and Fe_3O_4 has Tc = 858 K.

Fig. 24 M-H curve of the Gd_5Si_4 - Fe_3O_4 (S5) bilayer thin film heterostructure retains ferromagnetic behavior. The magnetic saturation (Ms) is about 3 emu. Transition temperatures are observed at around 243 K and 265 K. Note Gd_5Si_4 has Tc = 318 K and Fe_3O_4 has Tc = 858 K.

List of abbreviations

AFM - Atomic force microscopy

Ar - Argon

CA - Contrast agent

Fe_3O_4 - Iron (II, III) Oxide

FIB - Focused Ion Beam

Gd_5Si_4, Gd_5Si_3 and GdSi - Gadolinium silicide

GRE - Gradient echo

MNP - Magnetic nanoparticles

MRI - Magnetic resonance imaging

NP - Nanoparticles

NMR - Nuclear magnetic relaxation

RF - Radio-frequency

SEM - Scanning electron microscopy

SPION - Superparamagnetic Iron Oxide Nanopartilces

Tc - Curie / Transition temperature

TE - Echo time

TIG - Tungsten Inert Gas

TR - Repetition times

TSE - Turbo spin echo

XPS - Photo-electron spectroscopy

XRD - X-ray diffraction

Abstract

The motivation of this study is to investigate the size dependent properties of Gadolinium silicide nanoparticles and their potential applications in Biomedicine. We use two approaches in our investigation - size dependence and possible exchange interaction in a core-shell structure. Past results showed Gd_5Si_4 NPs exhibit significantly reduced echo time compared to superparamagnetic iron oxide nanoparticles (SPION) when measured in a 7 T magnetic resonance imaging (MRI) system. This indicates potential use of Gd_5Si_4 ferromagnetic nanoparticles as T2 contrast agents for MRI.

Until recently most contrast agents (CA) that are used in Magnetic Resonance Imaging (MRI) studies have been paramagnetic. However, ferromagnetic CAs are potentially more sensitive as T2 CAs than T1 paramagnetic compounds due to their large magnetic moments. Furthermore, the need for better MRI images without the need of upgrading to the higher magnetic field strength can be achieved using better CA such as Gd_5Si_4 NP. The quality of the image contrast in MRI is improved by shortening T1 and T2 relaxation times at the site or close proximity to the CA. In this study, effect of Gd_5Si_4 NP of varying sizes and with different concentrations are investigated on T1, T2 and T2* (effective/observed T2) relaxations times.

Further study was carried out on possible exchange interaction between Fe_3O_4 and Gd_5Si_4 to enhance the magnetic properties of the Gd_5Si_4 which could be later used to synthesize core-shell structures. Exchange interaction / bias is a phenomena associated with the exchange anisotropy created at the interface between the two magnetic materials. Therefore, thin films of varying thickness was deposited and studied for their magnetic properties.

Introduction

Early study of magnetic nanoparticles (MNPs) were motivated by geological and cultural heritage dating, while today's interest is focused mainly in biomedicine. Presently, biomedical field is a multidisciplinary area where research and development is largely focusing on applications in imaging, diagnostics and therapy. One of the most challenging problem in biomedicine is early detection of disease so that treatment could be delivered before the disease cause damage. Early biomedical imaging was done with X-rays, however imaging inside the organs was not possible since water and organic media provided little contrast within the tissue as they were transparent to X-rays. Therefore, new technologies were urgently needed.

MRI's for clinical applications were commercially introduced by GE in the 1980s [22]. In MRI, a strong magnetic field pulse is applied to a body causing water protons to be excited. The rate of the following relaxation is recorded and transferred into an image. The contrast between different tissues is determined by the rate at which excited atoms return to the equilibrium state. It was found that among other parameters, two major MRI parameters- spin relaxation time (T1) and lattice relaxation time (T2) of the water protons, could be affected by contrast agents (CA). The first MRI contrast agents were based on Gd complexes [27]. However, these are paramagnetic at body temperature. The signal-to-noise ratio can be significantly increased for NPs that are ferromagnetic. To enhance the contrast effect in MRI, MNPs are required to have optimum magnetic properties, which are strongly related to size, crystallinity, structure, and composition of MNPs.

A number of diagnosis methods based on MNPs are being developed for clinical use. The magnetism in nanoparticles is used due to their effect on nuclear magnetic relaxation (NMR) that is used to produce contrast enhancement in magnetic resonance imaging (MRI) images. In the last two decades, NP CAs have gained high importance in imaging and a large number are in preclinical testing and medical research [22].

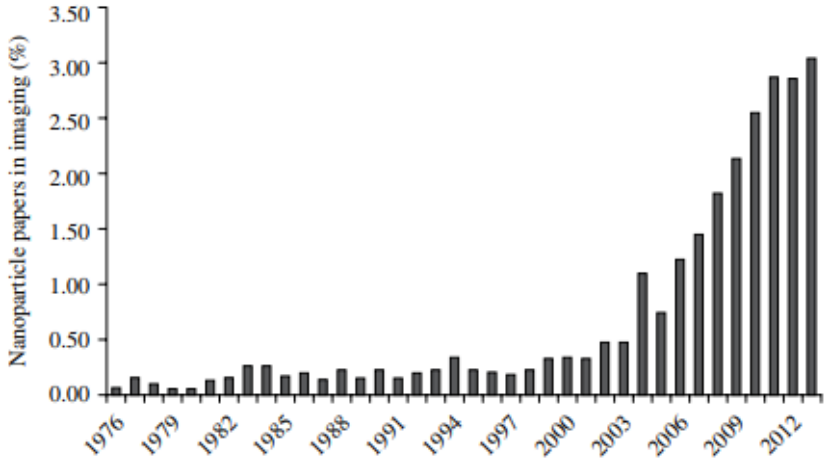

[22]Fig. 1 Growth of the nanoparticle research in biomedical imaging.

Fig. 2 Modern MRI machine with a image inset showing MRI brain images. (Source: GE Healthcare)

Size dependent properties

MNPs exhibit size-dependent magnetism. As the physical size of the specimen decreases from bulk to NP, an MNP shows a transition from multidomain structure to single-domain structure within, then the exchange forces may dominate and even in the presence of demagnetization energy, and the absence of any applied field, the particle is uniformly magnetized. The size at which the particle is single domain is called it's critical size, and is determined by the innate magnetic anisotropy energy of the material and usually falls in the range of tens of nanometers[24][25].

For a group of single-domain MNPs, their overall magnetization (M) reaches saturation (Ms) when their magnetization directions are aligned parallel to an applied magnetic field (H). The resistance to this magnetization alignment is measured by susceptibility (M/H). These magnetized NPs can retain some collective remnant magnetization even if the applied magnetic field is removed, similar to bulk ferromagnetic materials and reversing the external field in the opposite direction (coercive field / coercivity Hc), will fully demagnetize these MNPs. Further reduction of MNP size leads to superparamagnetism and the remnant magnetism drops to zero without applied magnetic field.

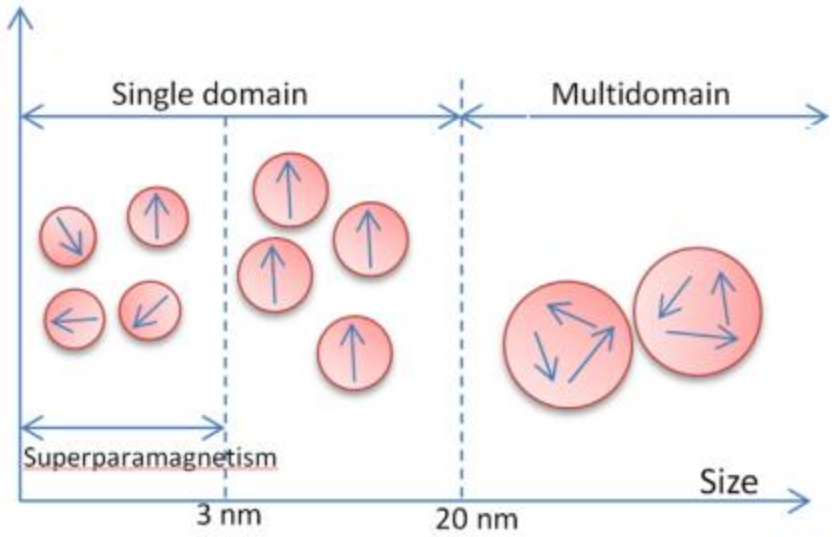

Fig. 3 Magnetic state of Magnetic nanoparticles as function of size [26].

MRI and Contrast agent

MRI works on the principal of nuclear magnetic relaxation (NMR) of water protons. When the magnetic field is applied, the protons align in two ways in an MRI scanner: parallel (low energy state) and antiparallel (high energy state). The population difference between these two states depends on the field strength. When the resonance electromagnetic radio-frequency (RF) pulse is applied perpendicular to the magnetic field direction, the protons absorb the energy and then jump to an antiparallel state. Subsequent removal of this RF irradiation causes spin to return to its equilibrium state — a process called *spin relaxation*. The process leading to moment increase in longitudinal direction is called *T1* relaxation, while that leading to moment decrease in transverse direction is called *T2* relaxation. These relaxation process are used to generate a bright (*T1* - *weighted*) and a dark (*T2* - *weighted*) image, respectively. The image contrast depends on local variation of relaxation time, resulting from the proton density and the physiological environment of specimen [27].

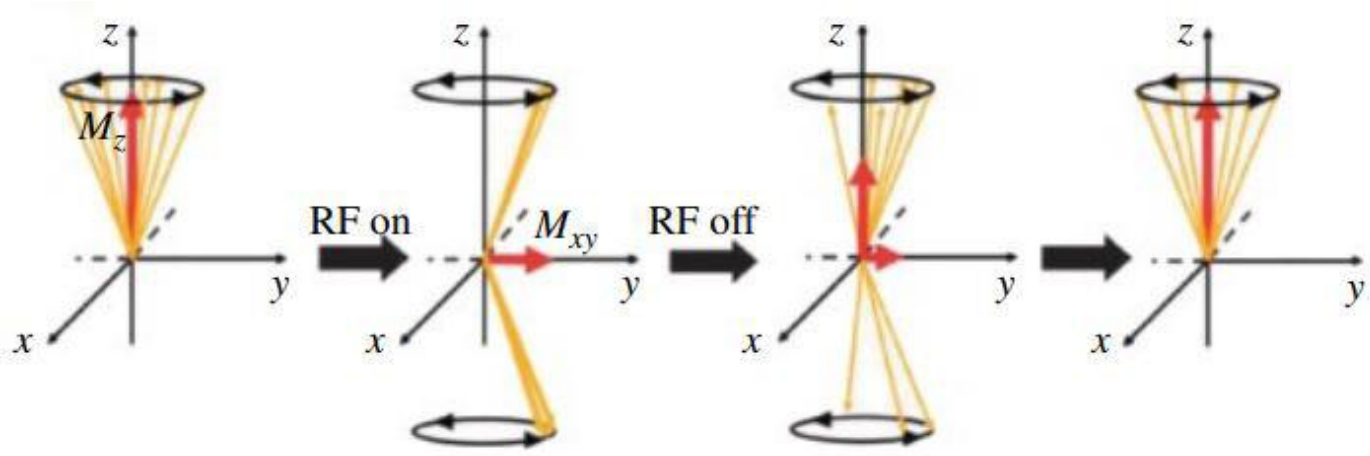

Fig. 4 Schematic illustrations of spin relaxation process of water protons [28].

Secondary magnetic field produced by MNPs can shorten the T2 of the surrounding protons. Therefore, MNPs can act as a *T2 contrast agent* (CA). The sensitivity of a T2 CA is given by the relaxation rate, **R2 = 1/T2** (s^{-1}) , and the relaxivity, **r2 = R2 / [concentration]** ($mM^{-1} \cdot s^{-1}$). The relaxation rate of the MNPs contrast agent in solution is given by,

$$\frac{1}{T_2} = \frac{\left(256\pi^2\gamma^2 / 405\right) V^* M_s^2 r^2}{D\left(1 + L / r\right)}$$

where γ is the proton gyromagnetic ratio, V* is the volume fraction, Ms is magnetic saturation, r is the radius of MNP core, D is the diffusivity of water molecules, and L is the thickness of an impermeable surface coating. Reading from the above equation, an MNP would make an ideal CA if it has high Ms, large r, and small L (thin coating). Furthermore, MNPs with narrow size distribution and an overall hydrodynamic size smaller than 50nm (long circulation time) [28][29].

Synthesis and ball-milling

Arc Melting is used for melting metals to synthesize alloys. A standard Tungsten Inert Gas (TIG) welding unit is used as a power source which initiates electric arc with the solid elements placed in a crucible in the copper hearth under argon atmosphere. Heat generated by the electric arc melts the elements to form alloy. The metals can be heated to a temperature in excess of 2000^{o}C. Many batches of alloys can be produced in a single evacuation depending on the available crucibles in the hearth. Amount of alloys also depends on the size of the crucible. There are three main parts to the system: power source, chiller and vacuum unit. The vacuum unit with rotary and diffusion pumps can attain a vacuum of 10^{6} mbar. The cold circulation water from the chiller cools both the copper hearth and the electrodes.

High energy Ball-milling is an top-down approach where a mechanical deformation process is used for producing nanopowders. The mechanical reduction of the particle size of a solid sample is done by crushing with one or more inert balls usually a ceramic, flint or stainless steel of 2-8 mm diameter, rotating at high speed of up to 650 rpm around a horizontal axis. A high-speed agitator is used to increase the speed of the balls which are held in vacuum or in an inert gas like Argon or Nitrogen. This process has been successfully used to produce metals with minimum particle sizes from 4 to 26 nm. This process has the advantage of being relatively inexpensive and can be easily scaled up to produce large quantities of material. However, a major concern of this technique is the contamination from milling balls and atmosphere which could be mitigated by the usages of surfactants, alloy-coated milling media, and inert atmospheres. A conventional high energy ball mill can initiate chemical reactions and structural changes in the sample during the process.

The synthesis process of Gd_5Si_4 NPs has been described in details by Hadimani et al. [4]. Gd_5Si_4 material was synthesized by arc-melting of the stoichiometric mixture of gadolinium and silicon on a water-cooled Cu-hearth under Ar atmosphere. To ensure homogeneity the sample was repeatedly arc melted six times. No further heat treatment was done on the as-cast sample. The as-cast bulk material is then grounded in an agate mortar and screened to obtain powders with particle size of 53 µm or smaller. To further reduce the particle size, the powder is then processed by high-energy ball milling in a magneto ball-mill (Uni-Ball-Mill 5) operating under high impact mode without adding any liquid processing agent. In a typical milling procedure, 4 g of bulk powder was milled with ~14.5 g of stainless-steel balls consisting of 2 balls of 11.1 mm diameter and 4 balls of 6.3 mm diameter. To prevent contamination with the metallic iron from the steel balls and the container, a milling time of 20 minutes was used. No further annealing of milled powders was performed before physical property measurements.

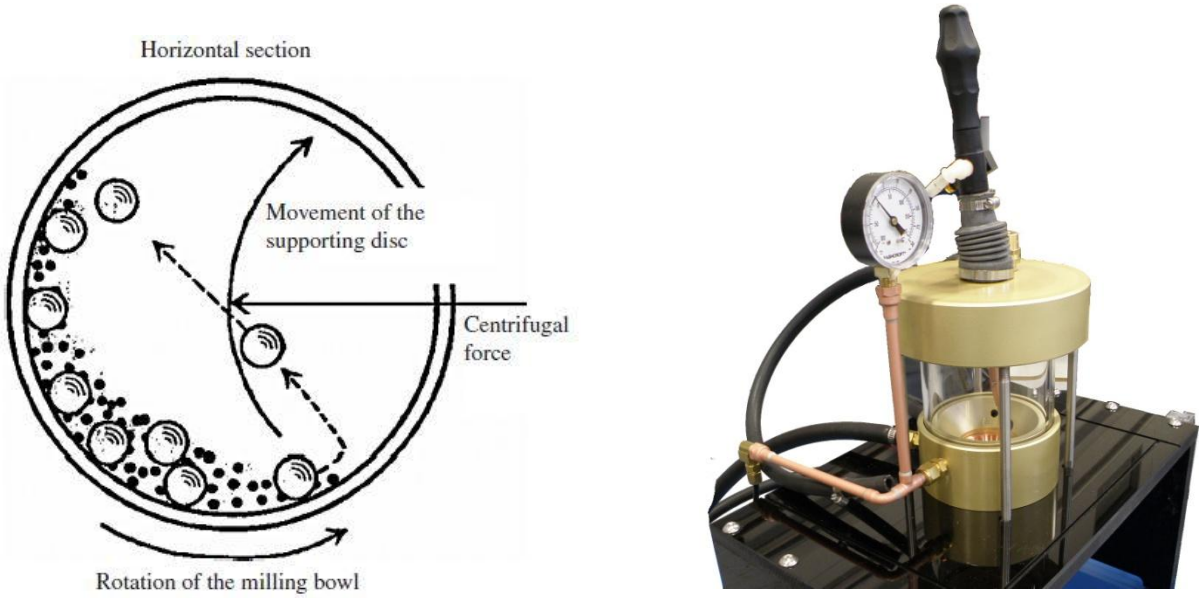

Fig. 5 (left) Schematic view of motion of the ball and powder mixture. (right) Arc melting system equipped with a single crucible in the copper hearth (source: Materials Research Furnaces) [21].

Properties of Gadolinium silicide - Gd_5Si_4, Gd_5Si_3 and GdSi

Gadolinium (electronic configuration: [Xe] 4f7 5d1 6s2) has the highest spin-only magnetic moment among all other atoms in the periodic table and has one of the lowest magnetocrystalline anisotropy among the rare-earths, making it a soft rare-earth ferromagnetic material close to room temperature [1]. Gadolinium ion (Gd3+) has seven unpaired electrons in its 4f orbitals, a high magnetic moment (μ2 = 63 BM2) and exhibit long proton spin-lattice relaxation time (T1 ≈ 10^{-9} sec) at field strengths routinely used in medical MRI (De León-Rodríguez 2015, Richards 1960). These unique properties resulted in chelated gadolinium complexes as being the most widely used T1 CA in MRI [18]. Since, these Gadolinium compounds are paramagnetic at human body temperature they are more suitable for use as T1 CA [4][23].

There are three identified phases of Gadolinium silicide in the NPs. Use of commercial grade precursors - Gd and Si leads to the formation of a smaller amount of Gd_5Si_3 and GdSi impurity in the predominantly Gd_5Si_4 matrix [3]. While Gd_5Si_4 is orthorhombic and ferromagnetic, Gd_5Si_3 and GdSi are paramagnetic at room temperture.

Methods and characterization

Methods are described in details elsewhere [18]. Briefly, Gadolinium silicide (Gd_5Si_4) was synthesized by arc-melting of the stoichiometric mixture of gadolinium and silicon under Ar atmosphere. Gd_5Si_4 NPs were then prepared by high energy ball milling of the crushed ingot. The synthesis process is described in detail elsewhere [4],[5],[6]. In order to separate NPs, one gram of the ball milled powder was added to 26 ml of ethyl alcohol. The suspension was sonicated for 4 hours to achieve thorough dispersion. Size separation was carried out by time sedimentation under applied dc magnetic field using NdFeB grade N52 permanent magnets placed below the beaker.

Eight fractions (S1, S2, S3, S4, S5, S6, S7 and S8) separation of 3.25 ml each of the suspension were extracted from the bottom after 3, 10, 45, 180, 600, 1440, and 4320 minutes of sedimentation, with the last fraction S8 being supernatant residue after the seventh extraction. After each extraction, the left over solution was sonicated for 30 minutes between S1 and S3 and 15 hours sonication for the rest in order to maintain good dispersion. The separated solutions were then evaporated at room temperature to obtain the powders. Magnetic properties were measured in vibrating sample magnetometer (VSM, Quantum Design Versalab) in a constant magnetic field of 100 Oe between 50Kand 350K and hysteresiswas measured in magnetic fields ranging -3T and 3T at 300 K.

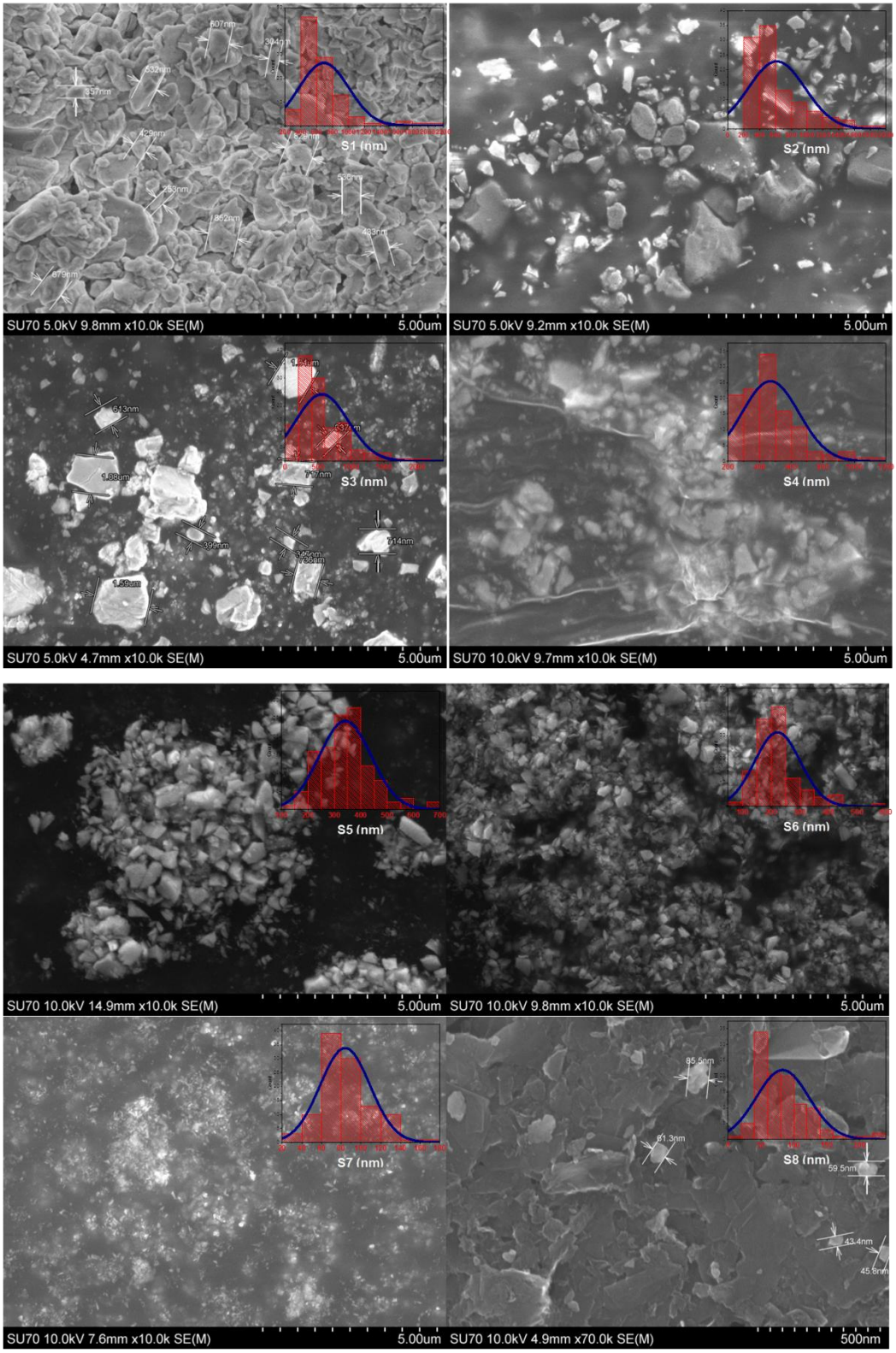

Fig. 6 SEM images of fractions. The figures inset shows average particle size distribution for each fraction [18].

The morphology and sizes of the NPs observed under Scanning Electron Microscopy (SEM Hitachi Su-70) show irregularly shaped NPs with definite size distribution within each fraction (refer Fig. 6). The average particle size distribution is determined by measuring the diameters of the particles individually using image analysis software from the SEM digital images. The figure inset with the SEM images display particle size distribution within each of those fractions.

Quantitative elemental analysis of the NPs was performed using spatially resolved energy dispersive X-ray spectroscopy (EDX), it confirms that there is no iron contamination in Gd_5Si_4 ingot from the production process (Fig. 7). X-ray diffraction (XRD) analysis (PANalytical X'Pert PRO) measurements indicate the presence of major phase Gd_5Si_4 and minor phase Gd_5Si_3 (Fig. 8). The obtained patterns for Gd_5Si_4 and Gd_5Si_3 are in good match with the reference peaks of

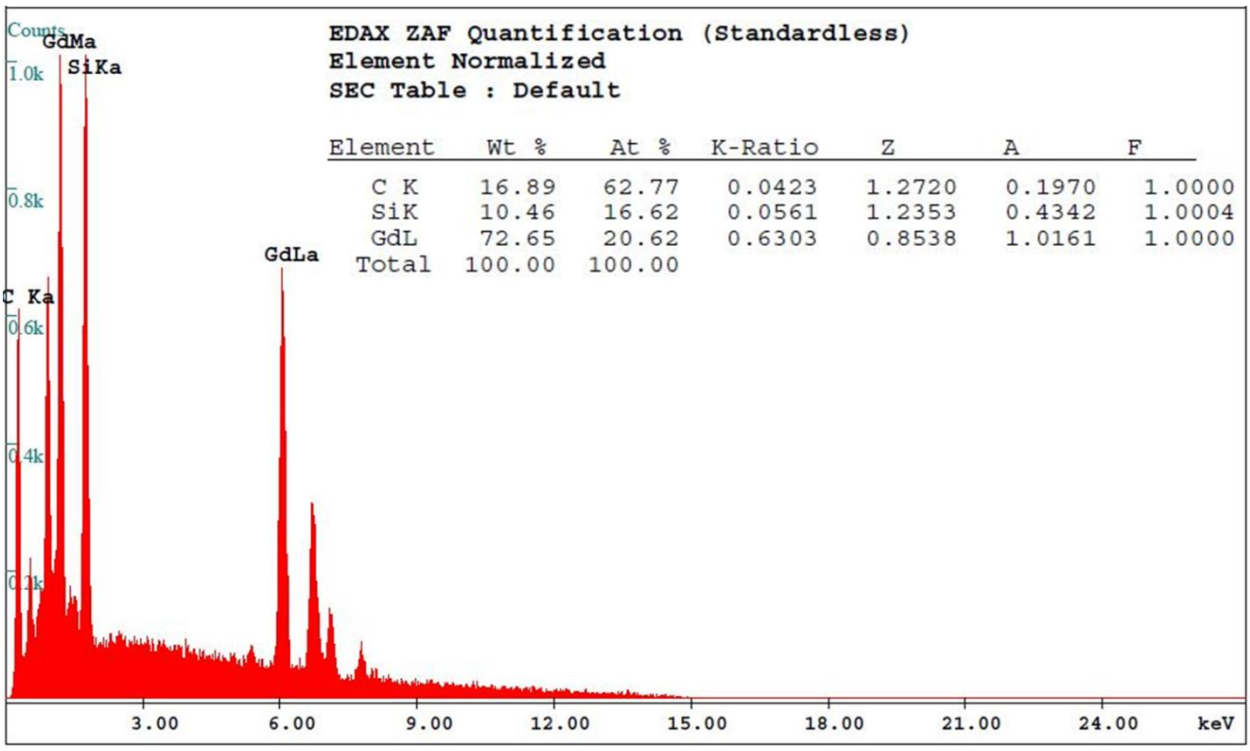

Fig. 7 Elemental analysis of a fraction (S3) in EDX [18]

the respective phases. The primary reference files for Gd_5Si_4 and Gd_5Si_3 matching reference peaks is sourced from "Calculated from ICSD using POWD-12++, (2004)" which are based on reported structure Refs. 15 and 16. The phase content in S7 and S8 fractions are largely amorphous. The deficit of Si in the particle has come from the bulk material. The bulk material was prepared by arc-melting which was reported in the reference number. The deficit in Si in the bulk material could have been a result of incongruent melting of Gd and Si elements in the arc-melter, difference in vapor pressures of the Gd and Si, splintering of individual elements in the arc-melting process due to uneven heat transfer and low thermal conductivity of Gd and Si [18].

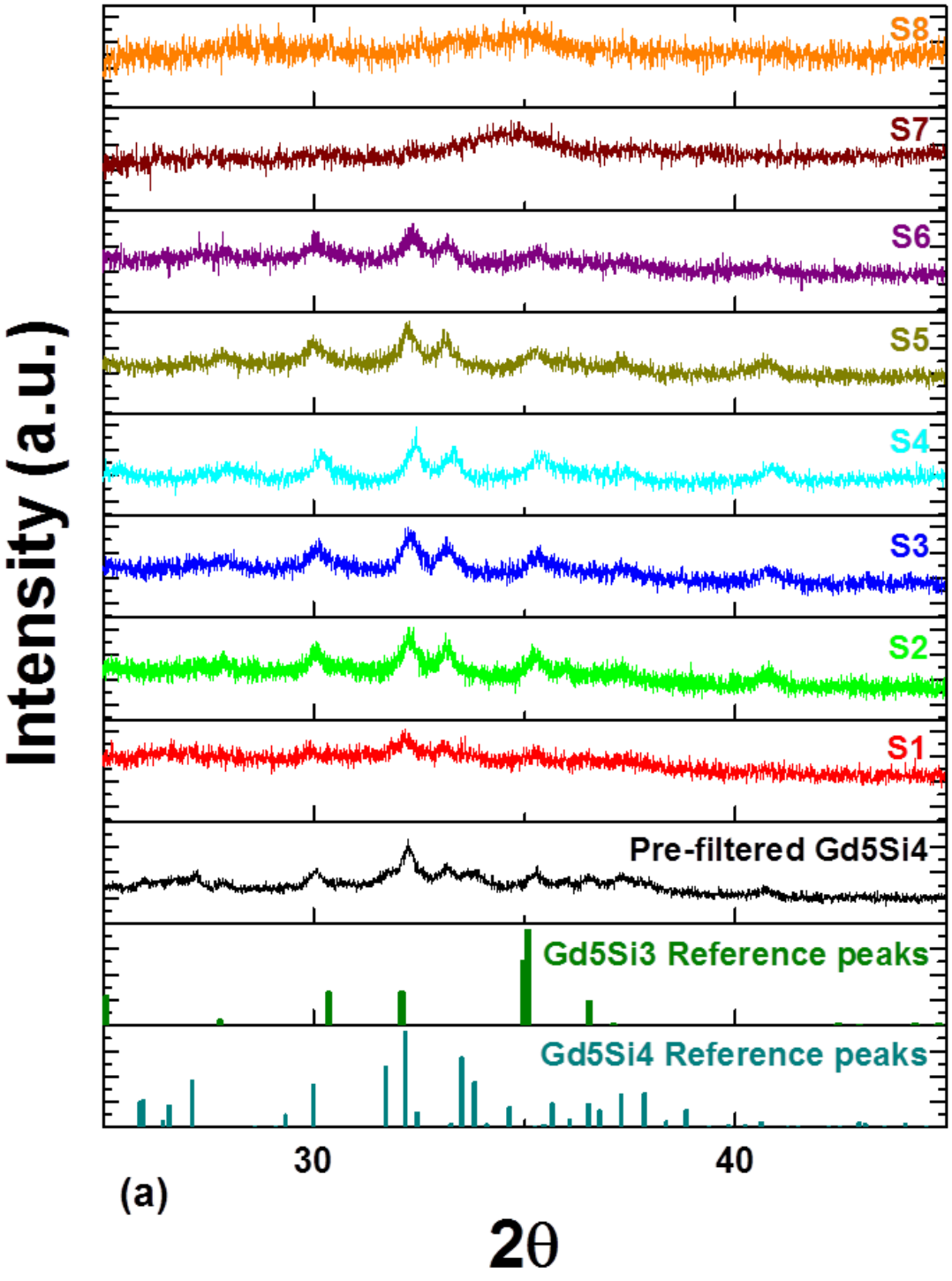

Fig. 8 (a) XRD patterns obtained from fractions. Reference peaks of Gd_5Si_4 and Gd_5Si_3 (bottom) matches with the patterns [18].

Fractions	Average particles size (nm)	Standard error
S1	688.30	30.71
S2	615.60	35.40
S3	555.54	36.15
S4	468.23	16.80
S5	341.15	8.97
S6	222	7.11
S7	83.84	2.43
S8	82.89	3.81

Standard error of the mean = Standard deviation / √(Sample size)

(b)

Table. 8 (b) Average particle sizes decrease across fractions [18].

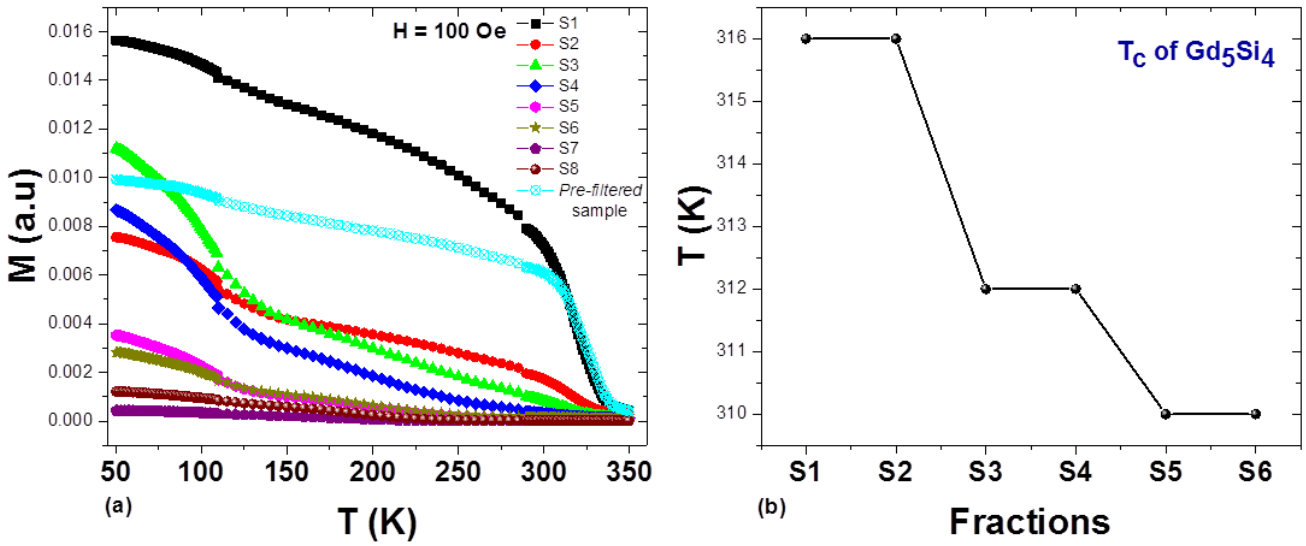

Fig. 9 (a) M-T curve for all fractions and pre-filtered sample (b) Curie temperatures (Tc) for each fraction (S1-S6) Gd_5Si_4 powder[18].

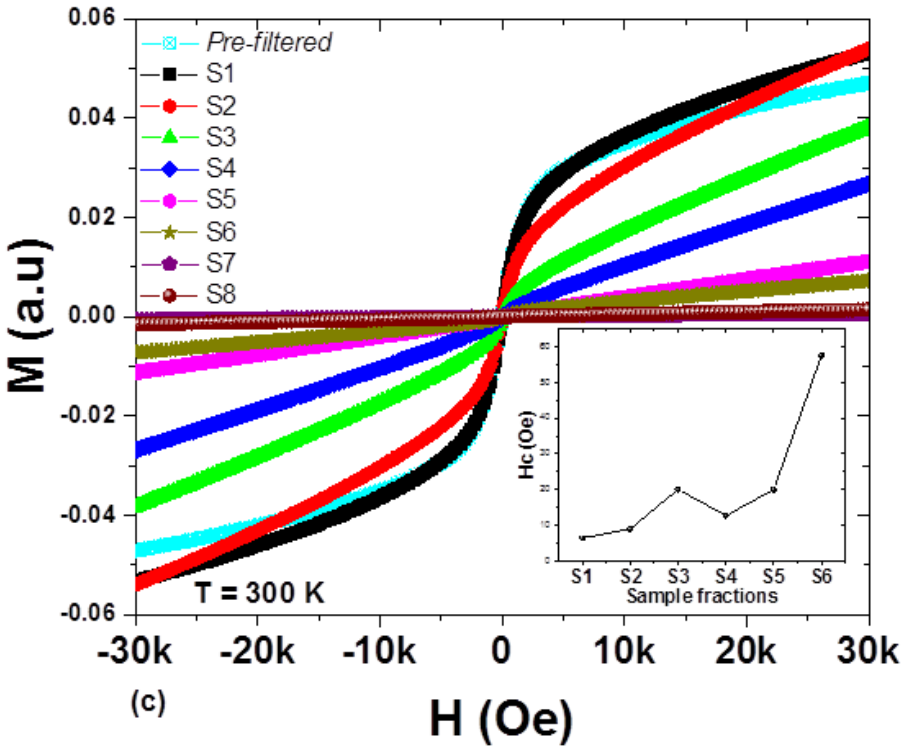

Fig. 9 (c) M-H curve for all fractions and pre-filtered sample; the figure inset showing coercivity (Hc) with respect to fractions. [18].

The magnetization as a function of temperature measurements indicate descending transition temperature for Gd_5Si_4 phase from 316 K for S1, S2 to 312 K for S3, S4 to 310 K for S5, S6 (Fig. 9(a)(b)). Fractions S7 and S8 shows no presence of Gd_5Si_4 phase which supports with XRD analysis.

The Tc of all the present phases in the fractions are determined by the intersection point of the steepest tangent (dM/dT) to the M-T curve with the T axis. Tc is observed at 110 K in all separation stages indicating presence of Gd_5Si_3 phase with the volume fraction of this phase

increasing in subsequent fractions at the expense of Gd_5Si_4 phase. This is inferred from a qualitative observation made by comparison of the approximate analysis of heights of the M-T curve at the curie temperatures of the respective phases. The increase in Tc of Gd_5Si_3 from 70 K at its bulk form to 110 K in powdered form also reported by Hadimani et al. [4] needs further exploration in order to fundamentally understand the cause for the significant shift in its Curie temperature. Another Curie temperature is observed at 290 K for all fractions indicating the presence of minuscule amount of elemental gadolinium. Presence of elemental gadolinium in the samples may be counter-intuitive as it oxidizes in oxygen rich environments however, the gadolinium oxide forms a barrier shell on the surface preventing further oxidation. Hence, gadolinium can be detected in our M-T measurements. The M-H curves at 300 K exhibits ferromagnetic behavior descending to paramagnetic as we move from S1 to S8 fraction. Coercivity (Hc) obtained from hysteresis plots show (inset of Fig. 9(c)) that it increases with decrease in particle size across fractions. This agrees with reports in the literature, where the coercivity increases with decrease in particle size until it reaches single domain and then decreases toward zero where it becomes superparamagnetic [18].

MRI studies

Advancing MRI magnetic technology is necessary for high resolution in biomedical imaging, high detection sensitivity and development of new classes of nanomaterials for use as CAs. CAs that are used in MRI today are mostly based on paramagnetic chelated gadolinium compounds as T1 CAs or superparamagnetic iron oxides (Fe_3O_4) as T2 CAs. Also, available CAs have limited effectiveness in high magnetic fields [31]. Until recently most CA that are used in MRI studies have been paramagnetic. However, ferromagnetic CAs are potentially more sensitive as T2 CAs than T1 paramagnetic compounds due to their large magnetic moments. Previous study has shown that ferromagnetic Gd_5Si_4 NP could be a better T2 CA for MRI with significantly reduced echo time (TE) compared to Superparamagnetic Iron Oxide Nanopartilces (SPION) which are currently the most widely used T2 CA [1]. Furthermore, the need for better MRI images without the need of upgrading to the higher magnetic field strength can be achieved using better CA such as Gd_5Si_4 NP. The quality of the image contrast in MRI is improved by shortening T1 and T2 relaxation times at the site or close proximity to the CA. The efficiency of a T1 CA is defined by its relaxivity, r1, which is field and temperature dependent. While, T2 agents are defined by their relaxivity, r2, which is dependent on both the saturation magnetization (Ms) value and the effective radius of the NPs [1, 2]. Here, effect of Gd_5Si_4 NP of varying sizes and with different concentrations are investigated on T1, T2 and T2* (effective/observed T2) relaxations times of proton using high field (21.1 T) MRI.

Prior to MRI measurements, NPs are diluted in solution with low-temperature 2% agarose with the following dilutions - 1:20, 1:200, 1:2000 and 1:20000. The high dilution factors were chosen

based on solution MRI with lower dilution factors (data not shown) that exhibited extremely strong contrast at 21.1 T and unquantifiable results. Each nanoparticle layer was separated with a 1% agarose layer. MR images were acquired on the 21.1 T (900 MHz) magnet at the National High Magnetic Field Laboratory (NHMFL) in Tallahassee, FL. The magnet is equipped with Bruker Avance III console and Paravision 6.0.1 (Bruker, Ettlingen Germany). For all acquisition a 10-mm birdcage coil was used together with a 63-mm (inner diameter) gradients capable of producing a peak gradient strength of 600 mT/m (Resonance Research Inc., Billerica MA). Measurements were performed to quantify T_1, T_2 and T_2* relaxation times for each sample and dilution. For T_1 measurements, a turbo spin echo (TSE) sequence was used with two rare factors. The echo time (TE) was 8.8 ms and ten incrementing (12000 - 26 ms) repetition times (TR) were used. T_2 relaxation were acquired with a multi slice multi echo (MSME) sequence using a TR=5000 ms and 20 incrementing echo time (7.5 – 150 ms). For T_2*, a 2D gradient echo (GRE) sequence were used with TR=5000ms and eight incrementing TE (1.5 – 28.5 ms). Common acquisition parameters for T_1 and T_2 sequences were 2 averages, matrix = 110x200, FOV = 1.1x 2.0 cm resulting in a 100x100 □m in plane resolution using a 1-mm slice while the 2D T_2* sequence were acquired with 2 averages and a matrix of 100x55 resulting in a 200x200 □m in-plane resolution. Magnitude images were analyzed in Paravision using region-of-interest (ROIs) to cover each agarose layer as well as spacing layers. The average signal intensities were extracted and analyzed in Matlab using the Levenberg-Marquardt algorithm. For T_1 a three-parameter exponential growth function were used while for T_2 and T_2* a three-parameter exponential decay function were employed.

The results indicate higher concentrations of NPs shortens the T2 and T2* relaxation times and the contrast disappears rapidly with any higher dilutions. Furthermore, fractions with higher

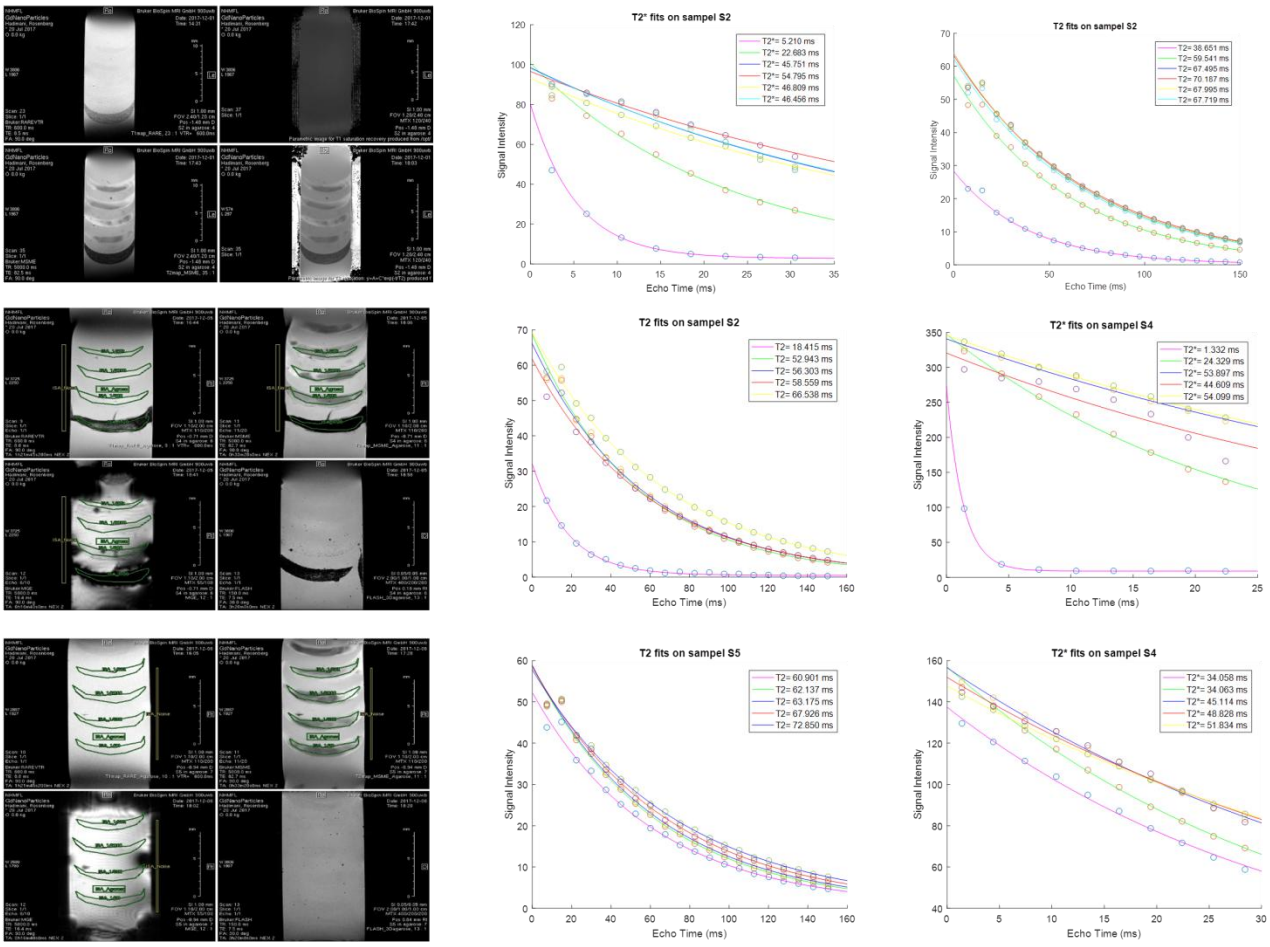

NPs ~ 586 nm			
Dilution in agarose	T1 (ms)	T2 (ms)	T2* (ms)
1/20	2436.0	38.7	5.2
1/200	2442.2	59.5	22.7
1/2000	2706.2	67.5	45.8
1/20000	2768.6	70.2	54.8
1/200000	2685.6	68.0	46.8
Agarose	2630.2	67.7	46.5

NPs ~ 287 nm			
Dilution in agarose	T1 (ms)	T2 (ms)	T2* (ms)
1/20	1365.9	18.4	1.3
1/200	1562.5	52.9	24.3
1/2000	1673.9	56.3	53.9
1/20000	1777.1	58.6	44.6
Agarose	1811.4	66.5	54.1

NPs ~ 135 nm			
Dilution in agarose	T1 (ms)	T2 (ms)	T2* (ms)
1/20	2438.6	63.4	34.1
1/200	2681.6	63.4	34.1
1/2000	2785.3	63.2	45.1
1/20000	2726.5	67.9	48.8
Agarose	2640.0	75.8	51.8

Fig. 10 MRI images of three fractions indicating T1, T2 and T2*. NPs are diluted in solution with low-temperature 2% agarose prior to MRI measurements at 21.1 T (900 MHz) magnet. (bottom) Table. - T1, T2 and T2* relaxation times of different NP sizes and at different concentrations.

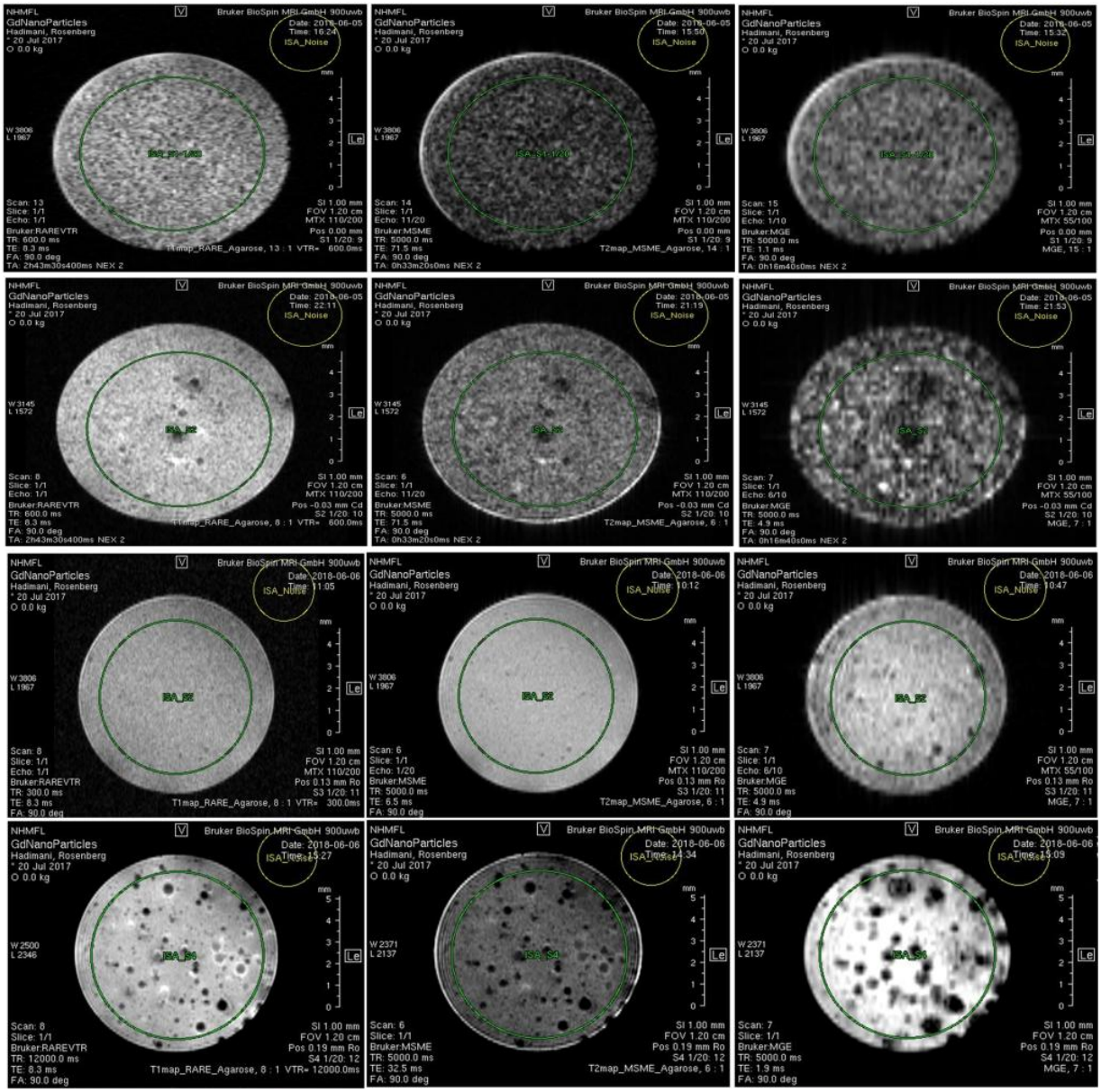

Sample #	T_1 (ms)	T_2 (ms)	T_2* (ms)
S1	3207.43	38.1704	**1.2187**
S2	3328.76	45.9614	**1.9925**
S3	3173.46	18.1262	**2.28242**
S4	3088.01	19.6214	**3.33331**

Fig. 11 - T_1, T_2 and T_2* MRI images and relaxation times of S1, S2, S3and S4 fractions.

ferromagnetic Gd_5Si_4 phase volume fraction and larger average particle size seems to have comparatively higher relaxation times than fractions with paramagnetic Gd_5Si_3 and GdSi phases. The results in Fig. 11 indicate effective T2 (T2*) decays much faster than the natural T2 suggesting large field inhomogeneities which could be caused by various factors such as imperfections in magnet or susceptibility effect induced field distortions from the material [30]. Furthermore, the measurements show decreasing NP sizes increases T2* relaxation time due to decrease in the net magnetization of the smaller particles resulting in longer T2*.

However, it should be noted that NPs have combination of all Gadolinium silicide phases present in them in different volume percentage. It is unknown how a NP with both ferromagnetic and paramagnetic components from different phases present in individual NPs affects the relaxation times of water protons. Therefore, further study is needed inorder to establish the cause in shortened relaxation times in smaller paramagnetic Gadolinium silicide (Gd_5Si_3 and GdSi) NPs and higher relaxation times in larger ferromagnetic Gadolinium silicide (Gd_5Si_4) NPs.

Magnetic properties of ferromagnetic Gd_5Si_4 - Fe_3O_4 bilayer thin film heterostructure

Introduction

Thin films are used in wide variety of high technology and industrial applications like data storage, batteries, sensors and microelectronics. There has been significant developments in magnetic thin films materials and fabrication in recent years. Thin films can be deposited with different processes such as spraying, spin-coating, dip-coating, chemical vapor deposition (CVD), evaporation, and sputtering.

Intrinsic magnetic properties such as magnetic saturation (Ms), Curie temperature (Tc) etc can be significantly different in thin films and in the bulk due to finite size effect [32]. Furthermore, it has been observed an exchange interaction results at the interface between a ferromagnetic material and an anti-ferromagnetic / ferrimagnetic material [33][34]. The exchange bias appears when the curie temperature of the ferromagnet is above the Neel temperature of the anti-ferromagnet / ferrimagnet [33]. This phenomena is exploited in data storage technology. In this paper we present deposition of Fe_3O_4 and Gd_5Si_4 films using RF Magnetron sputtering. Although Fe_3O_4 deposition with RF/DC sputtering has been widely reported, Gd_5Si_4 thin film deposition with this method has never been reported thus far.

Fe_3O_4 has an inverse spinel crystal structure with two cation sites- Fe^{2+} and Fe^{3+} ions that are encircled by oxygen ions to form tetrahedra and octahedra structures. Fe_3O_4 is ferrimagnetic whose magnetic property is influenced by the Fe^{2+} and Fe^{3+} ions as the spin of these ions at these two cation sites are anti-parallel coupled by super-exchange effect. Fe_3O_4 is reported to

exhibit high Curie temperature (~860 K) [4]. Gd_5Si_4 is ferromagnetic material with a reported transition temperature for PLD deposited thin film at 342 K [36]. It has an orthorhombic structure [37].

Methods

The samples were deposited on silicon substrate using RF magnetron sputtering using a pure Fe_3O_4 and Gd_5Si_4 ceramic targets. The apparatus is lab assembled unit equipped with RF generator, and a pumping system composed of a mechanical pump coupled with a turbo molecular pump. The base pressure of the growth chamber was on the order of 4×10^{-6} Torr. The apparatus is lab assembled unit equipped with RF generator, and a pumping system composed of a mechanical pump coupled with a turbo molecular pump. The distance between the target and the substrates was 55 mm and the RF power supply was set at 80 W for Fe_3O_4 deposition and 40 W for Gd_5Si_4 deposition. RF bias power densities of 0 W/cm2 were applied to the substrate. The gas used in this study was argon and the working pressure was kept at a value of 12 mTorr and 37 mTorr respectively. The flow was kept constant at a rate of 20 sccm for Fe_3O_4 and 25 sccm for Gd_5Si_4. Initial deposit was made with Fe_3O_4 followed by a top layer of Gd_5Si_4 to complete the bilayer structure. The surface roughness of this both layers was measured by atomic force microscopy. Furthermore, five samples of varying thickness of monolayers were deposited separately: 3 Fe_3O_4 films of deposition times of 15 minutes (*S1*), 30 minutes (*S2*) and 60 minutes (*S3*) and 2 Fe_3O_4 - Gd_5Si_4 bilayer films of deposition times of 30 minutes for Fe_3O_4 and 1 hour of Gd_5Si_4 (*S4*) and 1 hour each of Fe_3O_4 followed by Gd_5Si_4 (*S5*). Film thicknesses were measured using a Zeiss Auriga Crossbeam FIB - SEM dual system. Part of

the film was removed from top down to the substrate and the film thickness was thus measured with the sample slanted. Phase composition of the films were studied with PHI VersaProbe III Scanning XPS system. Morphology and microstructure of the as-deposited samples were examined by Dimension FastScan atomic force microscopy (AFM) and Hitachi SU-70 S/TEM. Finally, Magnetic properties were characterized with Quantum design Physical Property Measurement System (PPMS) system.

Fig. 12 RF / DC Magnetron system used for sputter deposition of the films.

Results and discussion

To observe the thicknesses, the samples were first coated with Pt in order to protect the specimens surface during milling. Then the specimens were milled to upto 5 µm depth using a Zeiss Auriga focused ion beam (FIB). The FIB milling voltage is set to 2 kV to minimize damage from implanted Ga. Specimens observed under SEM shows (Fig. 13) films thicknesses of 58 nm for *S1*, 96 nm for *S2*, 228.91 nm for *S3*, 83 nm of Fe_3O_4 and 90 nm of Gd_5Si_4 for *S4* and finally 110 nm of Fe_3O_4 and 175 nm of Gd_5Si_4 for S5. The thickness of the films are linearly proportional to the deposition times provided other parameters in the RF Magnetron sputtering remains the same.

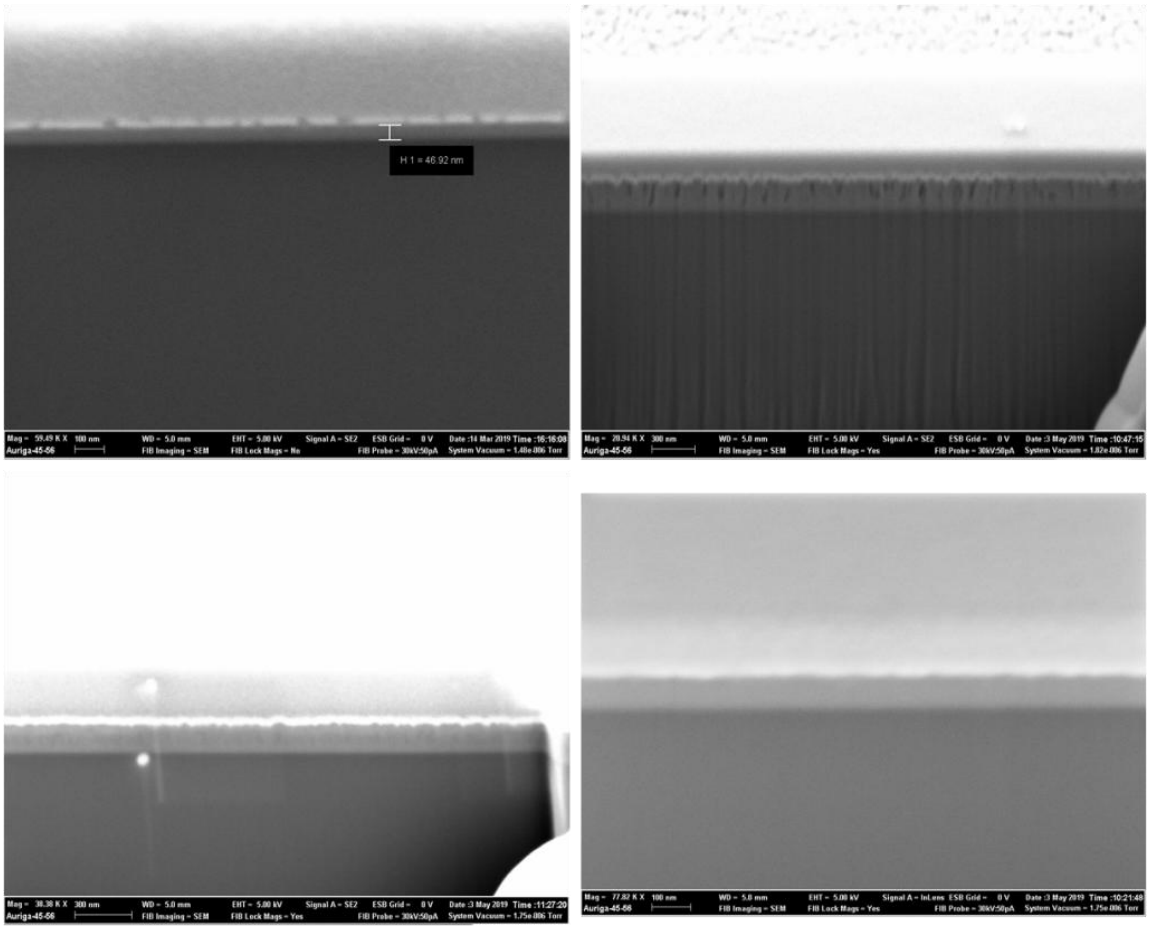

Fig. 13 SEM images of the specimen S1 - S4 (viewed at 54^o angle). The bright top layer is the protective Pt layer and the darker bottom layer is the silicon substrate.

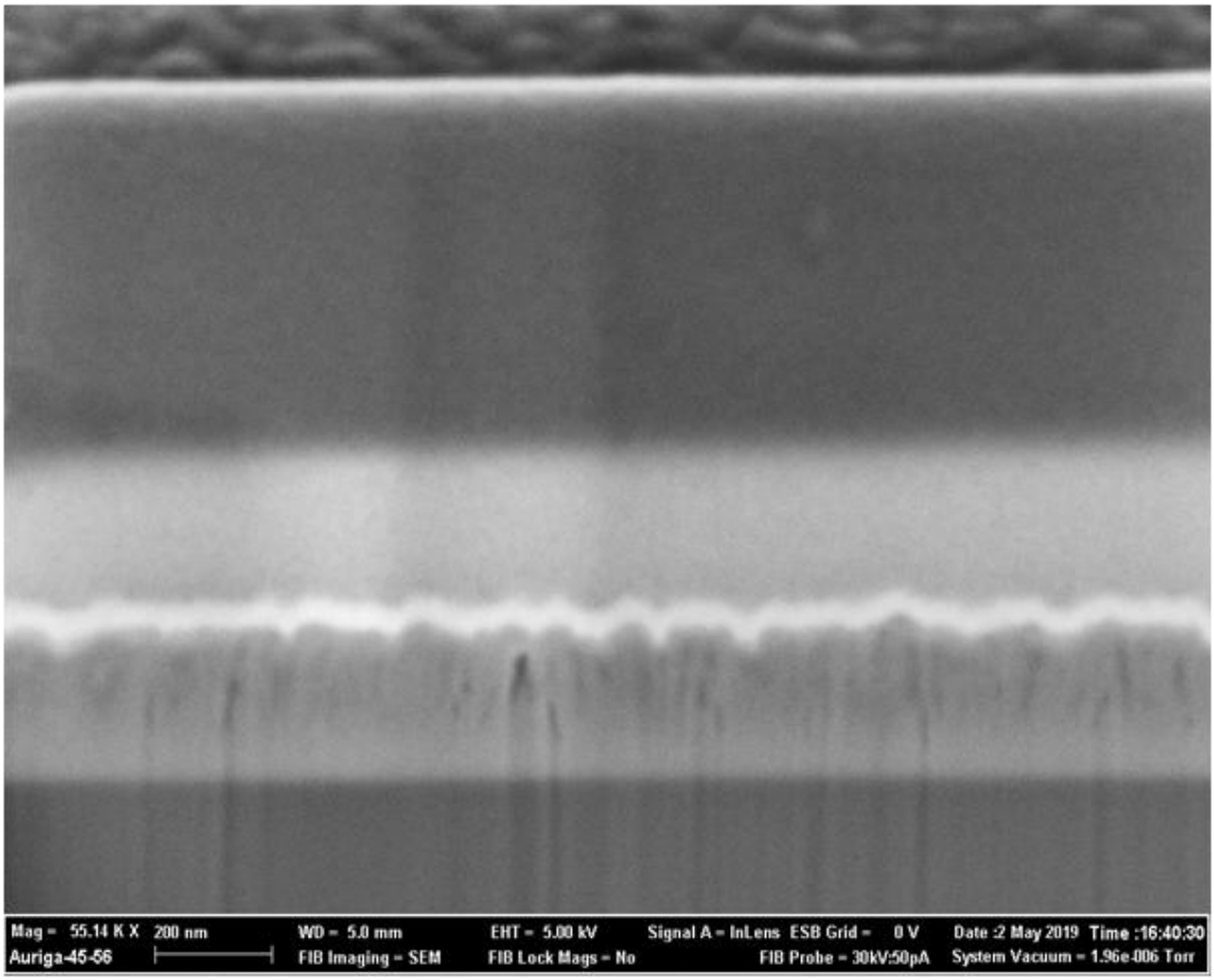

Fig. 14 SEM image of the specimen S5. Note contrast visible at the interface between the Pt layer on top and the silicon substrate. Gd_5Si_4 is deposited on Fe_3O_4.

The roughness of the both the Fe_3O_4 and Gd_5Si_4 film surface was found to be 0.738 nm, and 3.02 nm, respectively, as measured by atomic force microscopy (AFM), shown in Fig. 15 and Fig. 16. Silicon wafer used as the substrate in this experiment and its surface is regarded to be "flat". Interfacial topographies and surface morphology observed in SEM and AFM reveals non-homogeneous thickness in films and also significant void fraction in Gd_5Si_4 film. During growth, stress relaxation in between film interfaces strongly alters growth characteristics of the

following film deposition [43]. The respective surface roughness esp. at the interfacial layer will influence the global magnetic interaction as the physical contact area between two rough surface will depend on the roughness. Therefore, the amount of disorder at the surface/interface can also influences magnetic properties of thin magnetic films, such as coercivity, magnetic domain structure, and magnetization reversal. Also, surface/interface

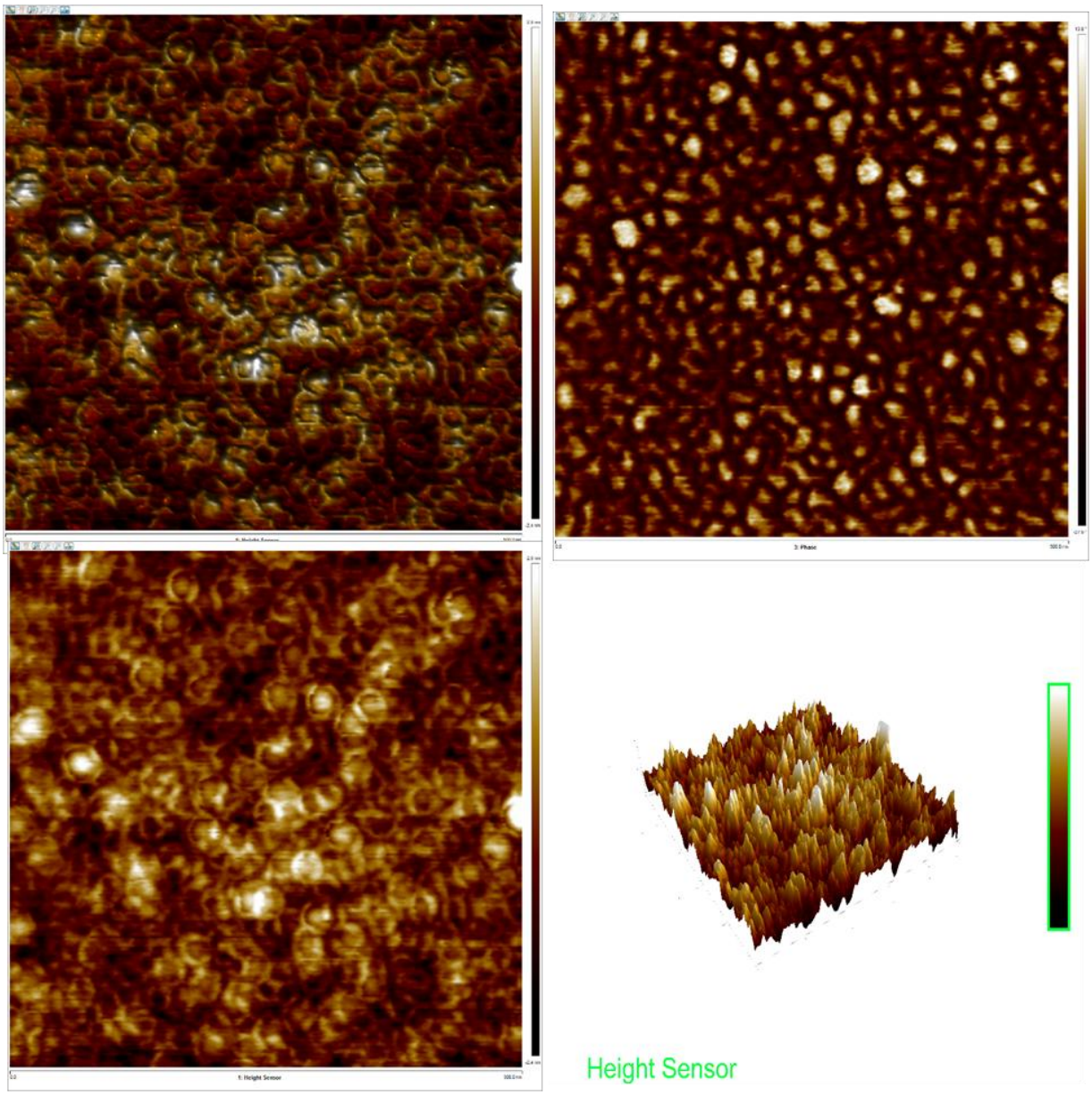

Fig. 15 AFM images (Height, Phase and 3D) of the Fe_3O_4 thin film shows surface roughness of **7.38 nm**. The surface roughness was analyzed with Nanoscope analysis software.

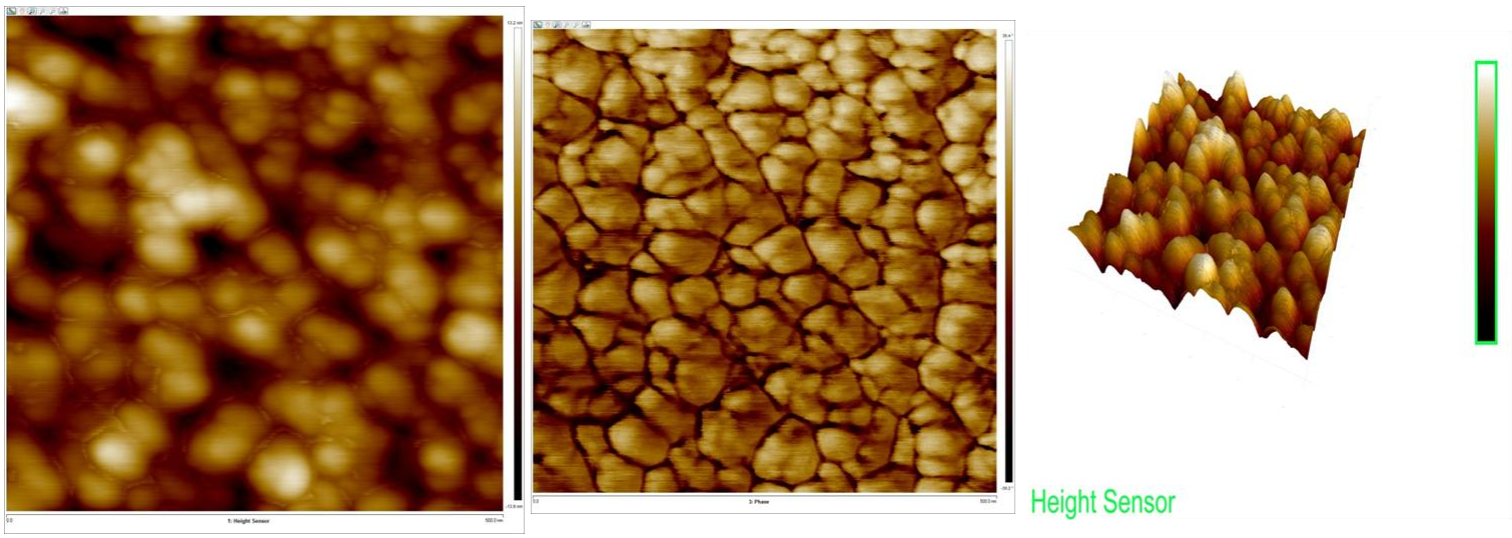

Fig. 16 AFM images (Height, Phase and 3D) of the Fe_3O_4 - Gd_5Si_4 thin film. Analysis shows surface roughness of **3.02 nm**.

roughness has been shown to have a significant influence on the demagnetizing field [43][44].

XPS surface characterization analysis shows elemental composition and phases. The XPS survey scan of the Fe_3O_4 thin film deposited on Si (100) substrate is shown in Fig. 16 , we have observed that only Fe and O are present with very small contribution of C which was expected because film surface was exposed to air before XPS measurements. The positions of various photoemission peaks are marked in the spectrum for elements present in the film. Further detailed scan have performed for Fe 2p core level spectra to determine charge/electronic state of elements present in the film.

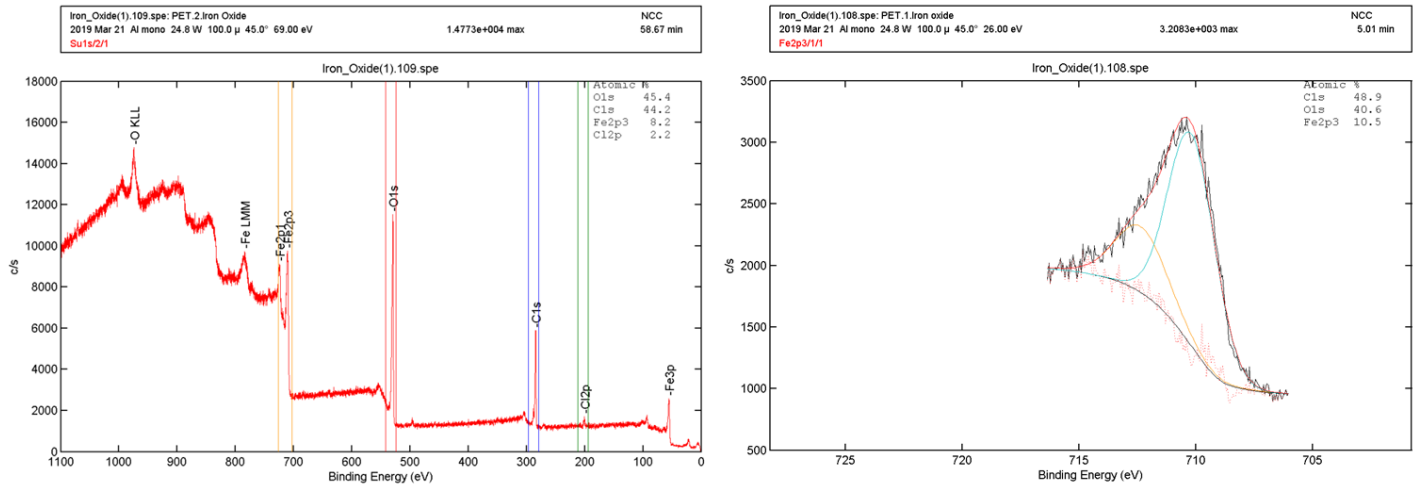

Fig. 17 XPS Survey spectrum of Fe_3O_4 film indicating presence of carbon. Analysis reveals presence of phases other than Fe_3O_4. (*right*) Fe_3O_4 (XPS SPECTRUM) - Region: Fe2p3 spectrum curve fitted to identify peaks.

Fig. 17 depicts the high-resolution scan of the Fe 2p core level. The deconvoluted spectrum shows the presence of two peaks at 710.18 eV attributed to Fe_3O_4 phase and 712.35 eV.

The survey scan of the Gd_5Si_4 deposited on Fe_3O_4 is shown in Fig. 18 Gd 4d core-level XPS spectrum of thin film is shown in Fig. 18. The features of Gd are fitted with Gaussian–Lorentzian functions which reveals binding energies of 142.50 eV, 147.98 eV and 152.69 eV. O 1s core level spectra has binding energy position at around 531.42 eVand for the Si 2p binding energy at 101.51 eV. All XPS core level spectra were fitted using PHI MultiPak data reduction and interpretation software package.

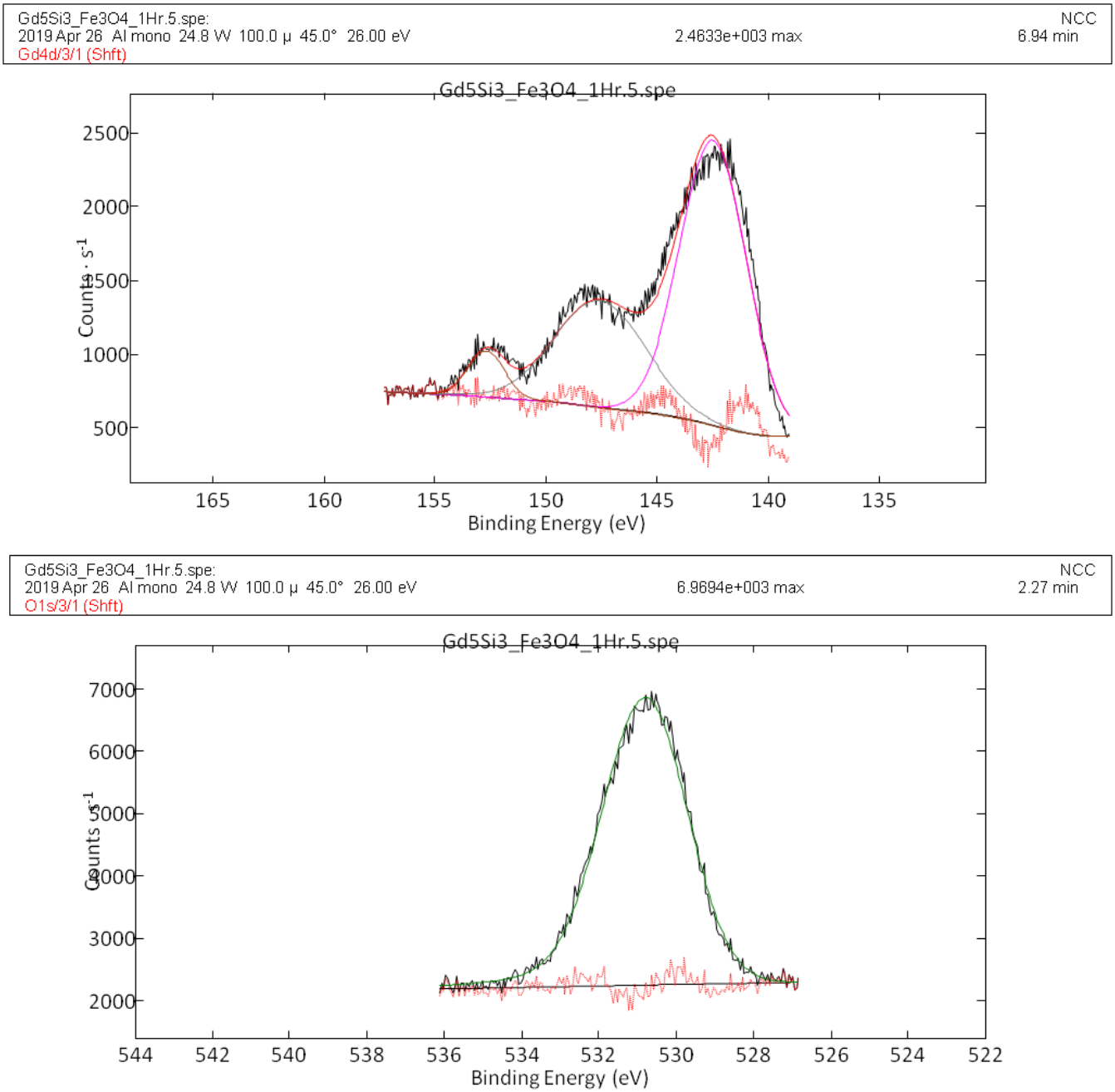

Fig. 18 XPS SPECTRUM - Region: Gd4d/3 spectrum curve fitted to identify peaks. (*bottom*) Region: O1s/3 spectrum curve fitted to identify peaks.

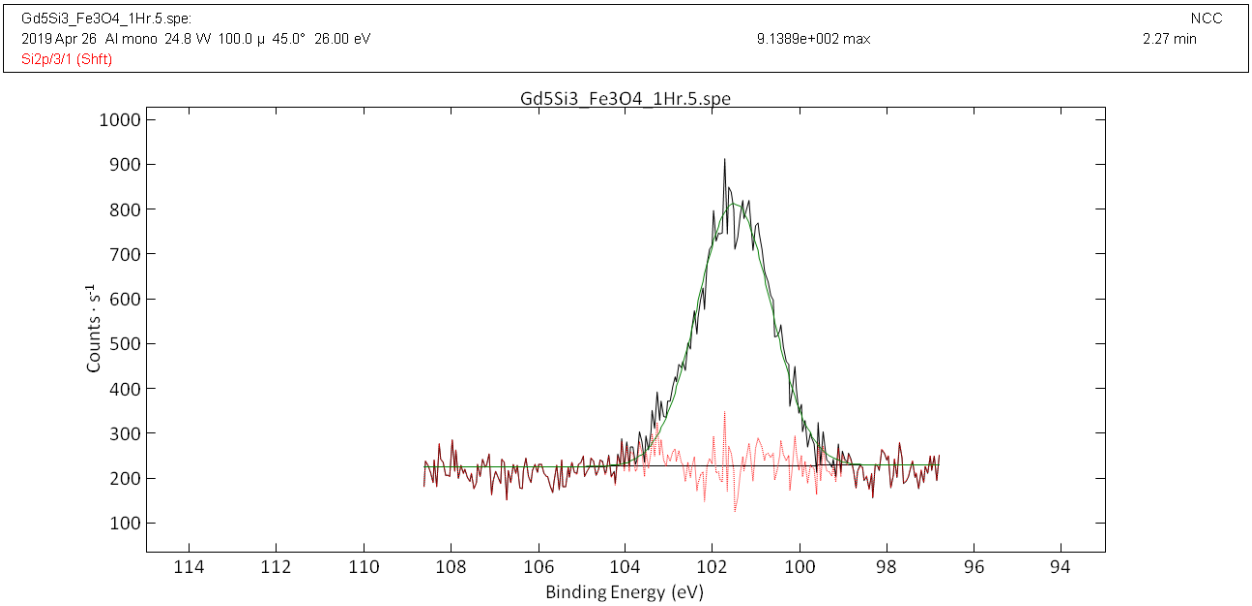

Fig. 19 XPS SPECTRUM - Region: Si2p/3 spectrum curve fitted to identify peaks.

The hysteresis (M-H) curves for the Fe_3O_4 thin films and Fe_3O_4/Gd_5Si_4 bilayer films are shown in Fig. 20, 21, 22, 23 and 24. The magnetic hysteresis plots of film at the room temperature and 50 K to 400 K were measured using QD PPMS. It can be seen that the Fe_3O_4 film deposited on glass substrate shows higher saturation magnetization (Ms = 8 emu), while the films deposited on Si(100) show lower saturation magnetizations (Ms = 2.6 emu for S1 and Ms = 2.9 emu for S2).

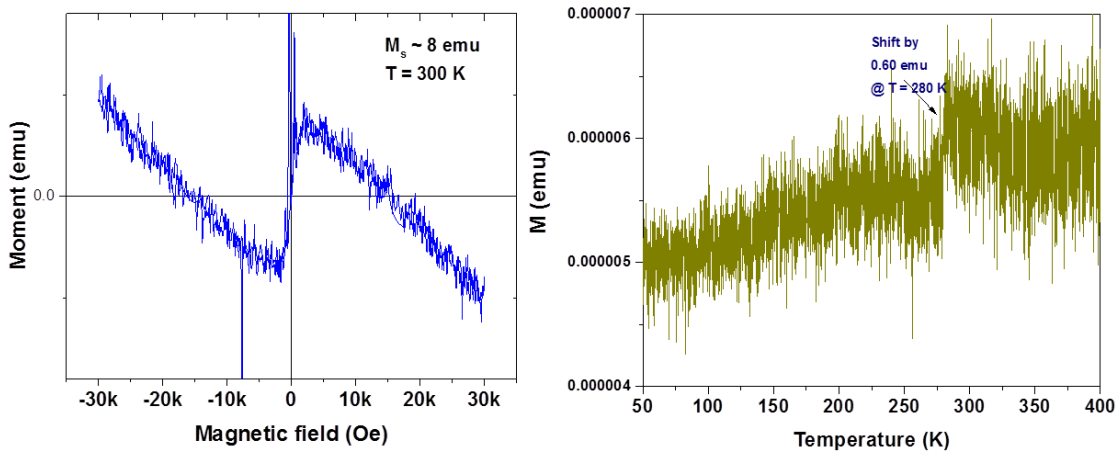

Fig. 20 Hysteresis graph of 58 nm thick Fe_3O_4 on glass. Fe_3O_4 (S1) thin film exhibit ferromagnetic behavior with magnetic saturation at around 8 emu. The diamagnetic features in

observed is due to glass/silicon substrate. (*right*) M-T Curve shows shift in moment by 0.60 emu at the temperature of 280K indicating possible transition.

This is because S1 is deposited on glass substrate while the S2 and S3 are deposited on Si(100), hence nature of the substrate surface plays a vital role in the synthesis of thin films and the inherent characteristics of substrate are very important [35][46]. Surface properties of glass and silicon have distinct influence on nucleation and growth processes of thin films [44]. There is large lattice mismatch of substrates (Si, a = 5.404 Å) and films (Fe_3O_4, a = 8.397 Å). The Curie temperature (Tc) was obtained from differentiating magnetic moments with respect to the temperature. Tc for Fe_3O_4 specimens were observed at 281 K for S1, 378 K for S2 and 300 K for S3.

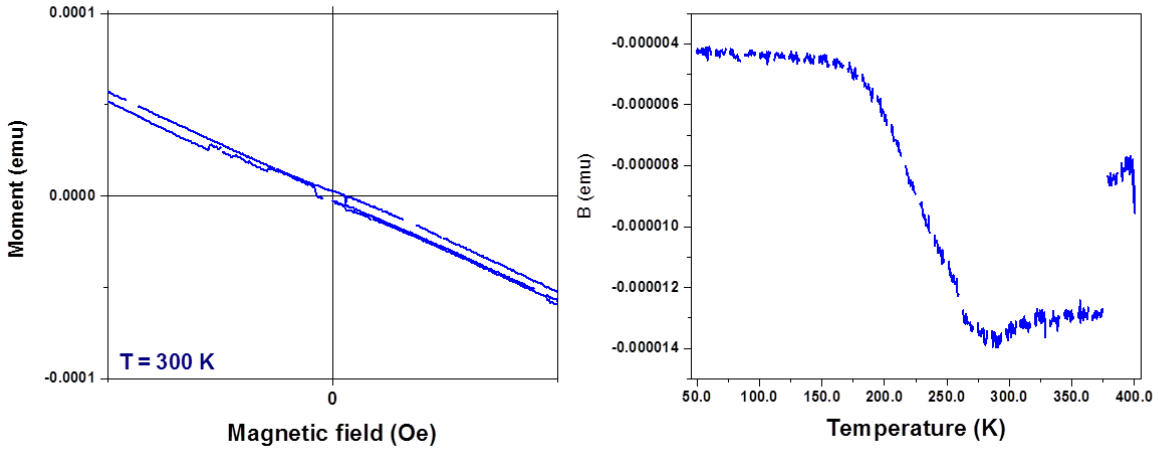

Fig. 21 M-H curve of the 96 nm thick Fe_3O_4 (S2) thin film on silicon showing magnetic saturation (Ms) at about 2.6 emu and Tc at 378 K.

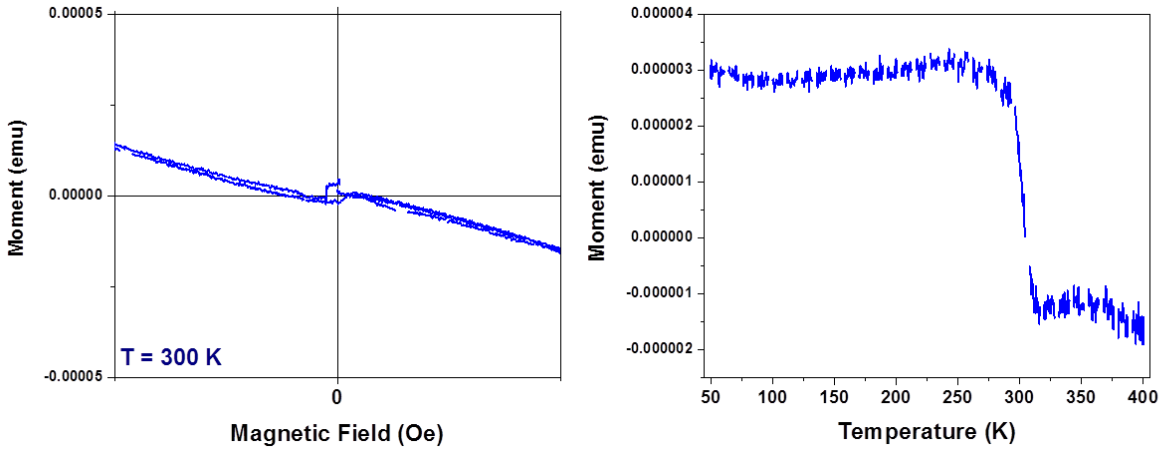

Fig. 22 M-H curve of the 228.91 nm thick Fe_3O_4 (S3) thin film on silicon showing magnetic saturation (Ms) at about 2.9 emu and Tc at about 300 K.

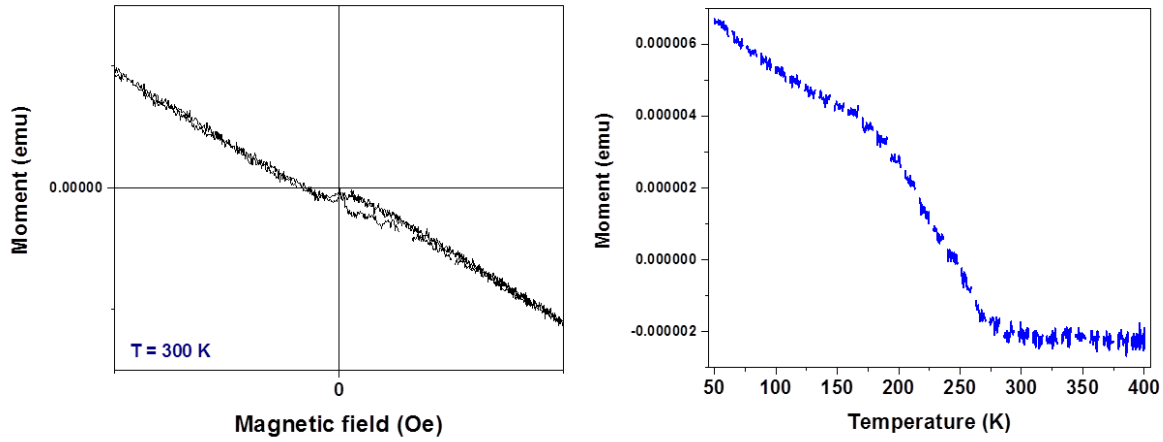

Fig. 23 M-H curve of the Gd_5Si_4 - Fe_3O_4 (S4) bilayer thin film heterostructure retains ferromagnetic behavior. The magnetic saturation (Ms) is about 1.58 emu. Transition temperatures are observed at around 148 K, 240 K and 300 K. Note Gd_5Si_4 has Tc = 318 K and Fe_3O_4 has Tc = 858 K [18][35].

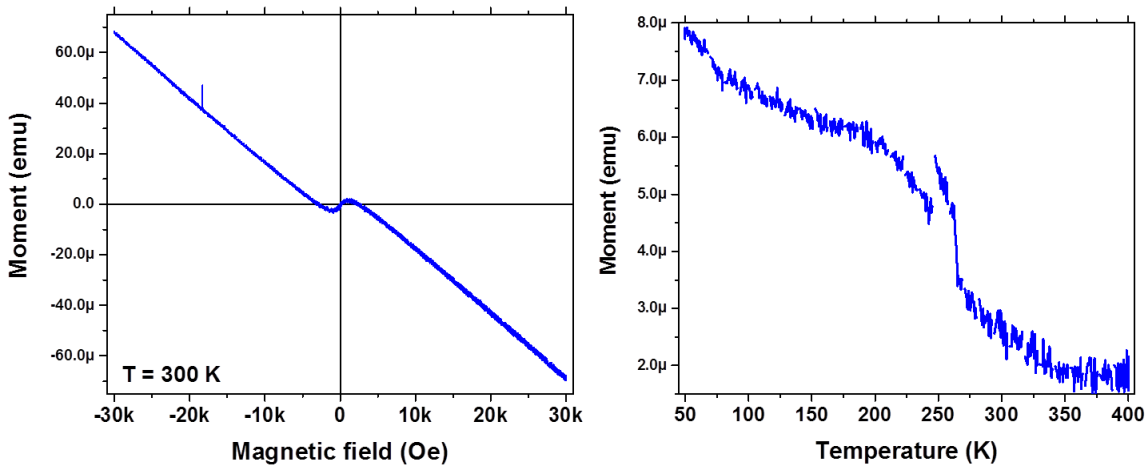

Fig. 24 M-H curve of the Gd_5Si_4 - Fe_3O_4 (S5) bilayer thin film heterostructure retains ferromagnetic behavior. The magnetic saturation (Ms) is about 3 emu. Transition temperatures are observed at around 243 K and 265 K. Note Gd_5Si_4 has Tc = 318 K and Fe_3O_4 has Tc = 858 K [18] [35].

Specimen S4 exhibited Tc at around 148 K, 240 K and 300 K while for S5 Tc is observed at 300 K and 378 K. Further work is under progress to understand the origin of these magnetic transitions. All magnetic measurements were carried out with specimens oriented 90° in respect of the direction of external magnetic field. It becomes evident, the missing characteristic signature in the shift of Curie temperatures observed in M-T curve that is between the curie temperatures of the bilayer materials [47], we conclude no exchange interaction was observed between Fe_3O_4 - Gd_5Si_4 bilayer film. This can be attributed to the formation of other phases due to possible reaction between the films and/or substrate and oxygen in the air, leading to changes in magnetic properties of the deposited materials.

Conclusion and future work

The phase and size separation of Gd_5Si_4 nanoparticles was successfully carried out with the time sensitive sedimentation technique under applied dc magnetic field using a N52 NdFeB permanent magnet. Average nanoparticle sizes decreased as the sedimentation time increased across fractions. Applying dc magnetic field in the separation process resulted in separation of phases (ferromagnetic Gd_5Si_4 phase from paramagnetic Gd_5Si_3 phase and other impurities). Curie temperature of major phase Gd_5Si_4 decreased from 316 K to 310 K across fractions indicating decrease in average Gd_5Si_4 particle sizes while the Curie temperature remained constant at 110 K and 290 K for Gd_5Si_3 phase and elemental gadolinium phase respectively being unaffected by particle size variation.

MRI studies indicate relaxation time increases with dilution and decreases with NP sizes with paramagnetic properties. Effective T2 (T2*) decays much faster than the natural T2 and decreasing NP sizes increases T2* relaxation time due to decrease in the net magnetization of the smaller particles resulting in longer T2*.

Future work should focus on further improvement on size separation method is required for e.g. with continous field flow fractionation to achieve monodispersity so that narrow particles size range is present in each size separated fractions. Also, sythesis process improvement is necessary to mitigate formation of other phases of Gd_5Si_4. Ball milling produces irregular shapes which has a different effect on relaxation time and hence shape control is also needed.

Also, Fe_3O_4 and Fe_3O_4-Gd_5Si_4 bilayer thin films of various thicknesses on Glass/Si (100) substrate by RF Magnetron sputtering technique have successfully been deposited. Our results indicate

magnetic property is dependent on substrate and thickness of the deposited material. There is an observation of high porosity and surface roughness in both the films. No exchange interaction was observed between Fe_3O_4-Gd_5Si_4 bilayer film due to formation of different phases. Further improvement in the deposition process is necessary to reduce surface roughness and promote larger physical contact to enhance magnetic interaction between the two layers. Also, phase preservation needs to be achieved for the deposited films.

References

[1] El-Gendy AA, Harstad SM, Vijayaragavan V, Gupta S, Pecharsky VK, Zweit J, Hadimani RL. "*Ferromagnetic Gd5Si4 Nanoparticles as T2 Contrast Agents for Magnetic Resonance Imaging*". IEEE Magnetics Letters 8, 1–4 (2017).

[2] Richards, R. et al, "*High resolution nuclear magnetic resonance*". Spectrochimica Acta 16, 244 (1960).

[3]H. Bin Na, I. C. Song, and T. Hyeon, "Inorganic nanoparticles for MRI contrast agents," *Adv. Mater.*, vol. 21, no. 21, pp. 2133–2148, (2009).

[4] R. L. Hadimani, S. Gupta, S. M. Harstad, V. K. Pecharsky, and D. C. Jiles, "Investigation of room temperature ferromagnetic nanoparticles of Gd5Si4," IEEE Trans. Mag. , vol. 51, p. 2504104, 2015.

[5]R. L. Hadimani et al, "*First Successful Fabrication of Nanoparticles of magnetocaloric Gd_5Si_4,*" Bull. Am. Phys. Soc., 60, (2015).

[6]R. Hadimani et al, *"Effect of Milling Time on the Blocking Temperature of Nanoparticles of Magnetocaloric Gd_5Si_4.* Bull. Am. Phys. Soc., (2016).

[7]S. Chikazumi, C. D. Graham. "*Physics of ferromagnetism*," Oxford University Press, (1997).

[8]K. M. Krishnan. "*Biomedical Nanomagnetics: A Spin Through Possibilities in Imaging, Diagnostics, and Therapy*," IEEE Trans. Magn., 46(7), 2523–2558, (2010).

[9]Omid Veiseh et al., "*Design and fabrication of magnetic nanoparticles for targeted drug delivery and imaging*," Advanced Drug Delivery Reviews. Volume 62, Issue 3, Pages 284-304**,** (2010)**.**

[10]Abolfazl Akbarzadeh et al., "*Magnetic nanoparticles: preparation, physical properties, and applications in biomedicine*," Nanoscale Res Lett., 7(1): 144. (2012).

[11]M. Angelakeris. "*Magnetic nanoparticles: A multifunctional vehicle for modern theranostics*," Biochimica et Biophysica Acta (BBA) - General Subjects Volume 1861, Issue 6, Pages 1642–1651, (2017).

[12] Harstad S, D'Souza N, Soin N, El-Gendy AA, Gupta S, Pecharsky VK, et al. Enhancement of *β* -phase in PVDF films embedded with ferromagnetic Gd5Si4 nanoparticles for piezoelectric energy harvesting. AIP Advances. 2017Apr;7(5):056411.

[13] Weinmann H, Brasch R, Press W, Wesbey G. Characteristics of gadolinium-DTPA complex: a potential NMR contrast agent. American Journal of Roentgenology. 1984;142(3):619–24

[14] Cabrera-García A, Vidal-Moya A, Bernabeu Á, Pacheco-Torres J, Checa-Chavarria E, Fernández E, et al. Gd-Si Oxide Nanoparticles as Contrast Agents in Magnetic Resonance Imaging. Nanomaterials. 2016Aug;6(6):109.

[15]Pecharsky, V.K. et al, *J. Alloys Compds.*, 260, 98, (1997).

[16]Roger, J., Yahia et al, *J. Solid State Chem*., 179, 2310, (2006).

[17]Fermon, Claude, and Marcel Van de Voorde. "*Nanomagnetism* Applications and Perspectives". Wiley-VCH, (2017).

[18] Hunagund, SG, Harstad, SM, El-Gendy, AA, Gupta, S, Pecharsky, VK, Hadimani RL, "Investigating phase transition temperatures of size separated gadolinium silicide magnetic nanoparticles". AIP Advances, (2017).

[19] León-Rodríguez LMD, Martins AF, Pinho MC, Rofsky NM, Sherry AD. Basic MR relaxation mechanisms and contrast agent design. Journal of Magnetic Resonance Imaging. 2015;42(3):545–65.

[20]Gupta, AK and Gupta, M. "Synthesis and surface engineering of iron oxide nanoparticles for biomedical applications". Biomaterials, 26(18), 3995–4021, 2005.

[21] W. Cao. Synthesis of Nanomaterials by High Energy Ball Milling. Skyspring Nanomaterials, Inc.

[22] M. Y. Berezin, Nanotechnology for biomedical imaging and diagnostics from nanoparticle design to clinical applications. Hoboken, NJ: Wiley, 2015.

[23] A. A. E. Gendy, R. L. Hadimani, and J. M. Barandiaran, Magnetic Nanostructured Materials: From Lab to Fab. Elsevier, 2018.

[24] Morrish AH. The Physical Principles of Magnetism. Volume 1, New York: Wiley-VCH; 2001.

[25] Skomski R, Coey J. Permanent Magnetism. Bristol: Institute of Physics Publishing; 1999.

[26] C. Fermon and M. H. van de Voorde, Nanomagnetism: applications and perspectives. Weinheim, Germany: Wiley-VCH, 2017.

[27] M. Y. Berezin, Nanotechnology for biomedical imaging and diagnostics from nanoparticle design to clinical applications. Hoboken, NJ: Wiley, 2015.

[28] H. B. Na and T. Hyeon, "MRI Contrast Agents Based on Inorganic Nanoparticles," Nanoplatform-Based Molecular Imaging, pp. 279–308, 2011.

[29] De León-Rodríguez, L. M. et al (2015). *"Basic MR relaxation mechanisms and contrast agent design."* Journal of Magnetic Resonance Imaging, 42(3), pp.545-565.

[30] Chavhan G.B. et al. *Principles, techniques, and applications of T2*-based MR imaging and its special applications*. Radiographics; 29:1433-1449 (2009).

[31] Rosenberg, J.T. et al. " *Intracellular MRI Contrast By SPIOs and Dy Chelates at 11.75 and 21.1 T* ". Proc. Intl. Soc. Mag. Reson. Med. 17 (2009).

[32] Nicola A. Spaldin, "Magnetic materials: Fundamentals and Applications," 2nd edn. Cambridge university press, 2011.

[33] F. Canet, S. Mangin, C. Bellouard, and M. Piecuch, "Positive exchange bias in ferromagnetic-ferrimagnetic bilayers: FeSn/FeGd," Europhysics Letters (EPL), vol. 52, no. 5, pp. 594–600, 2000.

[34] P. M. Shameem and M. S. Kumar, "Training effect of the exchange bias in sputter deposited Fe 3 O 4 thin films with varying thickness," Journal of Magnetism and Magnetic Materials, vol. 458, pp. 241–252, Jul. 2018.

[35] Xiaoyi Wang, et al. "A review of Fe3O4 thin films: Synthesis, modification and applications," Journal of Materials Science & Technology, Volume 34, Issue 8, Pages 1259-1272, 2018.

[36] R. L. Hadimani, Y. Mudryk, T. E. Prost, V. K. Pecharsky, K. A. Gschneidner, and D. C. Jiles, "Growth and characterization of Pt-protected Gd5Si4 thin films," *Journal of Applied Physics*, vol. 115, no. 17, 2014.

[37] Raja Shehryar Ali, et al. Structural, Optical and Electrical Characterization of Fe3O4 Thin Films Prepared using PVD Magnetron Sputtering (RF), Materials Today: Proceedings, Volume 2, Issue 10, Part B, 2015.

[38] Kihara, Kuniaki; Matsumoto, Takeo; Imamura, Moritaka (1986). "Structural change of orthorhombic-Itridymite with temperature: A study based on second-order thermal-vibrational parameters". *Zeitschrift für Kristallographie*. **177** (1–2): 27–38.

[39] B. Mauvernay et al. Elaboration and characterization of Fe1–xO thin films sputter deposited from magnetite target. Thin Solid Films, Volume 515, Issue 16, 2007.

[40] D.J. Srolovitz, Act. Mater. 37, 621 (1989); G. Palasantzas and J. Th. M. De Hosson, Appl. Phys. Lett. 78, 3044 (2001).

[41] Ultrathin Magnetic Structures I and II, ed. by J. A. C. Bland and B. Heinrich (Springer, New York, 1994).

[42] Y.-P. Zhao, R.M. Gamache, G.-C. Wang, T.-M. Lu, G. Palasantzas, J.Th.M. De Hosson, J. Appl. Phys. 89, 13 25 (2001); Y. P. Zhao, G. Palasantzas, G. -C. Wang, T. -M. Lu, and J. Th. M. De Hosson, Phys. Rev. B 60, 1216 (1999).

[43] Sandeep Kumar, Ram Prakash, R.J. Choudhary, D.M. Phase, Structural, XPS and magnetic studies of pulsed laser deposited Fe doped Eu2O3 thin film, Materials Research Bulletin, Volume 70, 2015.

[44] M. Ohring, The materials science of thin films. San Diego, Calif: Academic Press, 2006.

[45] K. A. Jackson, Kinetic processes: crystal growth, diffusion, and phase transitions in materials. Weinheim: Wiley-VCH Verlag GmbH & Co. KGaA, 2012.

[46] Md. Nahid Akter Shafi, et al. Comparative Study of Magnetization of Co Thin Films Deposited on Glass, GaAs (001) and Si (001) Substrates. Int. J. Thin. Fil. Sci. Tec. 4, No. 3, 193-197 (2015).

[47] K. O'Grady, L.E. Fernandez-Outon, G. Vallejo-Fernandez, A new paradigm for exchange bias in polycrystalline thin films, Journal of Magnetism and Magnetic Materials, Volume 322, Issue 8, 2010.

[48] C. Pescher, J. Pierre, A. Ermolieff, C. Vannuffel, Magnetic properties of gadolinium silicide thin films produced by different fabrication processes, Thin Solid Films, Volume 278, Issues 1–2, 1996.

Appendix

NIST XPS database reference

General:	
Element:	Fe
Formula:	Fe3O4
XPS Formula:	
Name:	iron(II) diiron(III) tetraoxide
CAS Registry No:	1317-61-9
Classes:	catalyst, mineral, oxide
Citation:	
Author Name(s):	Tan B.J., Klabunde K.J., Sherwood P.M.A.
Journal:	Chem. Mater. 2, 186 (1990)
Data Processing:	
Data Type:	Photoelectron Line
Line Designation:	2p3/2
Quality of Data:	Adequate
Binding Energy (eV)	710.2
Energy Uncertainty:	0.2
Background Subtraction Method:	other
Peak Location Method:	data
Full Width at Half-maximum Intensity (eV):	4.8
Gaussian Width (eV):	
Lorentzian Width (eV):	
Measurement Information:	
Use of X-ray Monochromator:	No
Excitation Energy:	Mg
X-ray Energy:	
Overal Energy Resolution (eV):	
Calibration:	Other, Fe2p3 = 706.86
Charge Reference:	Adventitious carbon
Energy Scale Evalution:	Reliable, with one-point correction of energy scale
Specimen Information:	
Specimen:	
Method of Determining Specimen Composition:	
Method of Determining Specimen Crystallinity:	
Specimen Temperature (K):	300
Sample Quality:	Adequate

General:	
Element:	Si
Formula:	Gd5Si3
XPS Formula:	
Name:	pentagadolinium trisilicide
CAS Registry No:	12024-95-2
Classes:	IV semiconductor, lanthanide, rare earth, silicide
Citation:	
Author Name(s):	Puppin E., Lindau I., Abbati I.
Journal:	Solid State Commun. 77, 983 (1991)
Data Processing:	
Data Type:	Photoelectron Line
Line Designation:	2p
Quality of Data:	Adequate
Binding Energy (eV)	98.1
Energy Uncertainty:	0.05
Background Subtraction Method:	
Peak Location Method:	data
Full Width at Half-maximum Intensity (eV):	
Gaussian Width (eV):	
Lorentzian Width (eV):	
Measurement Information:	
Use of X-ray Monochromator:	No
Excitation Energy:	Mg
X-ray Energy:	
Overal Energy Resolution (eV):	
Calibration:	FL = Fermi level
Charge Reference:	Conductor
Energy Scale Evalution:	Reliable (reported energy within 300 eV of a reference energy)
Specimen Information:	
Specimen:	polycrystalline, scraped
Method of Determining Specimen Composition:	
Method of Determining Specimen Crystallinity:	X-ray Diffraction
Specimen Temperature (K):	300
Sample Quality:	Adequate
Comment:	
Notes:	The sample was prepared by melting pure elements.

General:	
Element:	Si
Formula:	Gd3Si5
XPS Formula:	
Name:	trigadolinium pentasilicide
CAS Registry No:	12435-34-6
Classes:	IV semiconductor, lanthanide, rare earth, silicide
Citation:	
Author Name(s):	Puppin E., Lindau I., Abbati I.
Journal:	Solid State Commun. 77, 983 (1991)
Data Processing:	
Data Type:	Photoelectron Line
Line Designation:	2p
Quality of Data:	Adequate
Binding Energy (eV)	98.9
Energy Uncertainty:	0.05
Background Subtraction Method:	
Peak Location Method:	data
Full Width at Half-maximum Intensity (eV):	
Gaussian Width (eV):	
Lorentzian Width (eV):	
Measurement Information:	
Use of X-ray Monochromator:	No
Excitation Energy:	Mg
X-ray Energy:	
Overal Energy Resolution (eV):	
Calibration:	FL = Fermi level
Charge Reference:	Conductor
Energy Scale Evalution:	Reliable (reported energy within 300 eV of a reference energy)
Specimen Information:	
Specimen:	polycrystalline, scraped
Method of Determining Specimen Composition:	
Method of Determining Specimen Crystallinity:	X-ray Diffraction
Specimen Temperature (K):	300
Sample Quality:	Adequate
Comment:	
Notes:	The sample was prepared by melting pure elements.

General:	
Element:	Si
Formula:	GdSi
XPS Formula:	
Name:	gadolinium silicide
CAS Registry No:	12024-82-7
Classes:	IV semiconductor, lanthanide, rare earth, silicide
Citation:	
Author Name(s):	Puppin E., Lindau I., Abbati I.
Journal:	Solid State Commun. 77, 983 (1991)
Data Processing:	
Data Type:	Photoelectron Line
Line Designation:	2p
Quality of Data:	Adequate
Binding Energy (eV)	98.6
Energy Uncertainty:	0.05
Background Subtraction Method:	
Peak Location Method:	data
Full Width at Half-maximum Intensity (eV):	
Gaussian Width (eV):	
Lorentzian Width (eV):	
Measurement Information:	
Use of X-ray Monochromator:	No
Excitation Energy:	Mg
X-ray Energy:	
Overal Energy Resolution (eV):	
Calibration:	FL = Fermi level
Charge Reference:	Conductor
Energy Scale Evalution:	Reliable (reported energy within 300 eV of a reference energy)
Specimen Information:	
Specimen:	polycrystalline, scraped
Method of Determining Specimen Composition:	
Method of Determining Specimen Crystallinity:	X-ray Diffraction
Specimen Temperature (K):	300
Sample Quality:	Adequate
Comment:	
Notes:	The sample was prepared by melting pure elements.

General:	
Element:	O
Formula:	Gd2O3
XPS Formula:	
Name:	gadolinium(III) trioxide
CAS Registry No:	12064629
Classes:	lanthanide, oxide, rare earth
Citation:	
Author Name(s):	Raiser D., Deville J.P.
Journal:	J. Electron Spectrosc. Relat. Phemon. 57, 91 (1991)
Data Processing:	
Data Type:	Photoelectron Line
Line Designation:	1s
Quality of Data:	
Binding Energy (eV)	531.4
Energy Uncertainty:	
Background Subtraction Method:	
Peak Location Method:	
Full Width at Half-maximum Intensity (eV):	
Gaussian Width (eV):	
Lorentzian Width (eV):	
Measurement Information:	
Use of X-ray Monochromator:	No
Excitation Energy:	
X-ray Energy:	
Overal Energy Resolution (eV):	
Calibration:	C1s=284.6
Charge Reference:	Adventitious carbon
Energy Scale Evalution:	Two-point correction of energy scale
Specimen Information:	
Specimen:	powder (when a special point is made in the article)
Method of Determining Specimen Composition:	
Method of Determining Specimen Crystallinity:	
Specimen Temperature (K):	
Sample Quality:	

General:	
Element:	Gd
Formula:	Gd5Si3
XPS Formula:	
Name:	pentagadolinium trisilicide
CAS Registry No:	12024-95-2
Classes:	IV semiconductor, lanthanide, rare earth, silicide
Citation:	
Author Name(s):	Puppin E., Lindau I., Abbati I.
Journal:	Solid State Commun. 77, 983 (1991)
Data Processing:	
Data Type:	Photoelectron Line
Line Designation:	4d5/2
Quality of Data:	Adequate
Binding Energy (eV)	141.6
Energy Uncertainty:	0.2
Background Subtraction Method:	
Peak Location Method:	data
Full Width at Half-maximum Intensity (eV):	
Gaussian Width (eV):	
Lorentzian Width (eV):	
Measurement Information:	
Use of X-ray Monochromator:	No
Excitation Energy:	Mg
X-ray Energy:	
Overal Energy Resolution (eV):	
Calibration:	FL = Fermi level
Charge Reference:	Conductor
Energy Scale Evalution:	Reliable (reported energy within 300 eV of a reference energy)
Specimen Information:	
Specimen:	polycrystalline, scraped
Method of Determining Specimen Composition:	
Method of Determining Specimen Crystallinity:	X-ray Diffraction
Specimen Temperature (K):	300
Sample Quality:	Adequate
Comment:	
Notes:	The sample was prepared by melting pure elements.

General:	
Element:	Gd
Formula:	GdSi
XPS Formula:	
Name:	gadolinium silicide
CAS Registry No:	12024-82-7
Classes:	IV semiconductor, lanthanide, rare earth, silicide
Citation:	
Author Name(s):	Puppin E., Lindau I., Abbati I.
Journal:	Solid State Commun. 77, 983 (1991)
Data Processing:	
Data Type:	Photoelectron Line
Line Designation:	4d5/2
Quality of Data:	Adequate
Binding Energy (eV)	141.5
Energy Uncertainty:	0.2
Background Subtraction Method:	
Peak Location Method:	data
Full Width at Half-maximum Intensity (eV):	
Gaussian Width (eV):	
Lorentzian Width (eV):	
Measurement Information:	
Use of X-ray Monochromator:	No
Excitation Energy:	Mg
X-ray Energy:	
Overal Energy Resolution (eV):	
Calibration:	FL = Fermi level
Charge Reference:	Conductor
Energy Scale Evalution:	Reliable (reported energy within 300 eV of a reference energy)
Specimen Information:	
Specimen:	polycrystalline, scraped
Method of Determining Specimen Composition:	
Method of Determining Specimen Crystallinity:	X-ray Diffraction
Specimen Temperature (K):	300
Sample Quality:	Adequate
Comment:	
Notes:	The sample was prepared by melting pure elements.

General:	
Element:	Gd
Formula:	Gd2O3
XPS Formula:	
Name:	gadolinium(III) trioxide
CAS Registry No:	12064629
Classes:	lanthanide, oxide, rare earth
Citation:	
Author Name(s):	Raiser D., Deville J.P.
Journal:	J. Electron Spectrosc. Relat. Phemon. 57, 91 (1991)
Data Processing:	
Data Type:	Photoelectron Line
Line Designation:	4d3/2
Quality of Data:	
Binding Energy (eV)	148.10
Energy Uncertainty:	
Background Subtraction Method:	
Peak Location Method:	
Full Width at Half-maximum Intensity (eV):	
Gaussian Width (eV):	
Lorentzian Width (eV):	
Measurement Information:	
Use of X-ray Monochromator:	No
Excitation Energy:	
X-ray Energy:	
Overal Energy Resolution (eV):	
Calibration:	C1s=284.6
Charge Reference:	Adventitious carbon
Energy Scale Evalution:	Two-point correction of energy scale
Specimen Information:	
Specimen:	powder (when a special point is made in the article)
Method of Determining Specimen Composition:	
Method of Determining Specimen Crystallinity:	
Specimen Temperature (K):	
Sample Quality:	

General:	
Element:	Gd
Formula:	Gd2O3
XPS Formula:	
Name:	gadolinium(III) trioxide
CAS Registry No:	12064629
Classes:	lanthanide, oxide, rare earth
Citation:	
Author Name(s):	Raiser D., Deville J.P.
Journal:	J. Electron Spectrosc. Relat. Phemon. 57, 91 (1991)
Data Processing:	
Data Type:	Photoelectron Line
Line Designation:	4d5/2
Quality of Data:	
Binding Energy (eV)	142.70
Energy Uncertainty:	
Background Subtraction Method:	
Peak Location Method:	
Full Width at Half-maximum Intensity (eV):	
Gaussian Width (eV):	
Lorentzian Width (eV):	
Measurement Information:	
Use of X-ray Monochromator:	No
Excitation Energy:	
X-ray Energy:	
Overal Energy Resolution (eV):	
Calibration:	C1s=284.6
Charge Reference:	Adventitious carbon
Energy Scale Evalution:	Two-point correction of energy scale
Specimen Information:	
Specimen:	powder (when a special point is made in the article)
Method of Determining Specimen Composition:	
Method of Determining Specimen Crystallinity:	
Specimen Temperature (K):	
Sample Quality:	

AIP ADVANCES 8, 056428 (2018)

Investigating phase transition temperatures of size separated gadolinium silicide magnetic nanoparticles

Shivakumar G. Hunagund,[1] Shane M. Harstad,[1] Ahmed A. El-Gendy,[2] Shalabh Gupta,[3] Vitalij K. Pecharsky,[3,4] and Ravi L. Hadimani[1,a]
[1]*Dept. of Mechanical and Nuclear Engineering, Virginia Commonwealth University, Richmond, VA 23284, USA*
[2]*Dept. of Physics, University of Texas at El Paso, El Paso, TX 79968, USA*
[3]*Ames Laboratory, US Dept. of Energy, Iowa State University, Ames, IA 50011, USA*
[4]*Dept. of Material Science and Engineering, Iowa State University, Ames, IA 50011, USA*

(Presented 9 November 2017; received 2 October 2017; accepted 22 November 2017; published online 11 January 2018)

Gadolinium silicide (Gd_5Si_4) nanoparticles (NPs) exhibit different properties compared to their parent bulk materials due to finite size, shape, and surface effects. NPs were prepared by high energy ball-milling of the as-cast Gd_5Si_4 ingot and size separated into eight fractions using time sensitive sedimentation in an applied dc magnetic field with average particle sizes ranging from 700 nm to 82 nm. The largest Gd_5Si_4 NPs order ferromagnetically at 316 K. A second anomaly observed at 110 K can be ascribed to a Gd_5Si_3 impurity. As the particle sizes decrease, the volume fraction of Gd_5Si_3 phase increases at the expense of the Gd_5Si_4 phase, and the ferromagnetic transition temperature of Gd_5Si_4 is reduced from 316 K to 310 K, while the ordering of the minor phase is independent of the particle size, remaining at 110 K.
https://doi.org/10.1063/1.5007686

INTRODUCTION

Elemental gadolinium (electronic configuration: [Xe] $4f^7\ 5d^1\ 6s^2$) has the largest spin-only magnetic moment among all other atoms in the periodic table.[1] Its trivalent ion Gd^{3+} with seven unpaired $4f$ electrons has long proton spin-lattice relaxation time (T1 $\approx 10^{-9}$ sec) at field strengths routinely used in medical Magnetic Resonance Imaging (MRI).[2] This unique feature of gadolinium resulted in chelated gadolinium complexes being the most widely used T1 contrast agents (CA) in MRI.[13] However, these compounds are paramagnetic at human body temperature making them suitable for use only as T1 CA.[4,14]

An alternative class of CA referred to as T2 is based on spin-spin relaxation process. Currently, superparamagnetic iron oxide nanoparticles (SPIONs) are beginning to be used as T2 CA. However, for continued improvement of biomedical imaging, there is an increasing need for improved CAs.[3] Ferromagnetic gadolinium silicide (Gd_5Si_4) nanoparticles are shown to be useful as potential T2 CA for MRI with significantly reduced echo time (TE) compared to SPIONs.[1] The production of the Gd_5Si_4 NPs via chemical synthesis routes has been challenging due to high oxygen affinity of gadolinium leading to significantly reduced magnetization. Therefore, top-down approach in an inert atmosphere is adopted not only to mitigate the oxidation of gadolinium but also increase yield through high scalability.

Furthermore, advances in nanotechnology are leading to the development of nanoscale materials with specifically engineered properties that differ from their bulk counterparts.[8] NPs pharmacokinetics *in vivo* are largely influenced by their physicochemical properties such as morphology, size and other surface properties.[9,11] The physicochemical properties in turn influence the magnetic behavior

[a]Email: rhadimani@vcu.edu

of individual NPs, since the magnetic properties of the NPs emerge from finite size and surface effects.[10]

High imaging performance of CAs in MRI depends on their increased relaxivity coefficients (*r1* and *r2*). In our recent publication we have shown that image contrast in MRI can be enhanced by higher saturation magnetization (M_s) of Gd_5Si_4 nanoparticles.[2] In this study, the size dependent magnetic properties of Gd_5Si_4 NPs are investigated.

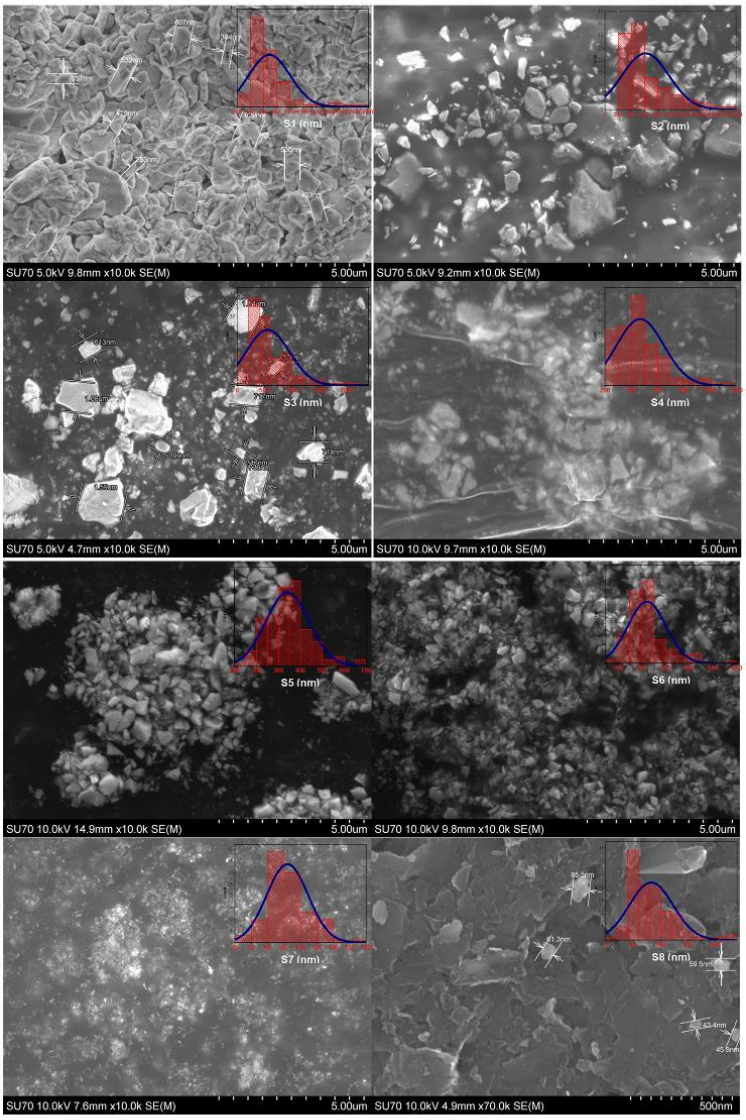

FIG. 1. SEM images of fractions. The figures inset shows average particle size distribution for each fraction.

METHODS

Gadolinium silicide (Gd_5Si_4) was synthesized by arc-melting of the stoichiometric mixture of gadolinium and silicon under Ar atmosphere. Gd_5Si_4 NPs were then prepared by high energy ball milling of the crushed ingot. The synthesis process is described in detail elsewhere.[5,6,12] In order to separate NPs, one gram of the ball milled powder was added to 26 ml of ethyl alcohol. The suspension was sonicated for 4 hours to achieve thorough dispersion. Size separation was carried out by time sedimentation under applied dc magnetic field using NdFeB grade N52 permanent magnets placed below the beaker. Eight fractions (*S1, S2, S3, S4, S5, S6, S7 and S8*) separation of 3.25 ml each of the suspension were extracted from the bottom after 3, 10, 45, 180, 600, 1440, and 4320 minutes of sedimentation, with the last fraction *S8* being supernatant residue after the seventh extraction. After each extraction, the left over solution was sonicated for 30 minutes between *S1* and *S3* and 15 hours sonication for the rest in order to maintain good dispersion. The separated solutions were then evaporated at room temperature to obtain the powders.

Magnetic properties were measured in vibrating sample magnetometer (VSM, Quantum Design Versalab) in a constant magnetic field of 100 Oe between 50 K and 350K and hysteresis was measured in magnetic fields ranging -3T and 3T at 300 K.

RESULTS AND DISCUSSION

The morphology of the nanoparticles was characterized by Scanning Electron Microscopy (SEM, Hitachi Su-70) and quantitative elemental analysis of the nanoparticles was performed using spatially resolved energy dispersive X-ray spectroscopy (EDX). The images reveal irregularly shaped NPs with certain size distribution within each fraction. The advantage of such irregular shaped NPs over spherical shaped ones are that they are found to have better pharmacokinetics and possibly greater cell binding affinity.[9] Diameters of the particles were individually measured using image analysis software (ImageJ) from the SEM digital images in order to determine the average particle size distribution. The resulting histogram is embedded with the SEM images of fractions. The SEM images show noticeable size variation along the fractions as shown in Fig. 1. EDX analysis confirms that there is no iron contamination in Gd_5Si_4 ingot from the production process (Fig. 2). X-ray diffraction (XRD) analysis (PANalytical X'Pert PRO) measurements reveal (Fig. 3) the presence of major phase Gd_5Si_4 and minor phase Gd_5Si_3. The obtained patterns for Gd_5Si_4 and Gd_5Si_3 are in good match with the reference peaks of the respective phases. The primary reference files for Gd_5Si_4 and Gd_5Si_3 matching reference peaks is sourced from "*Calculated from ICSD using POWD-12++*, (2004)" which are based on reported structure Refs. 15 and 16. The phase content in *S7* and *S8*

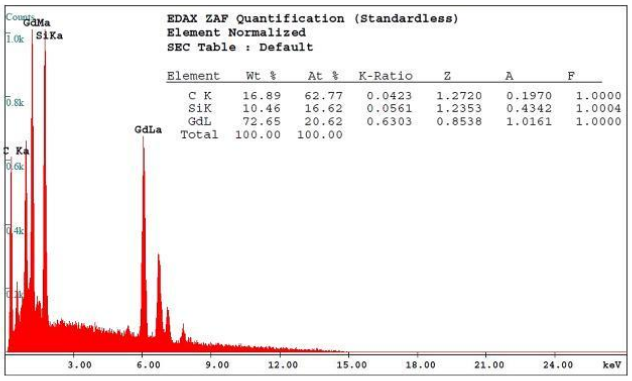

FIG. 2. Elemental analysis of a fraction (*S3*) in EDX.

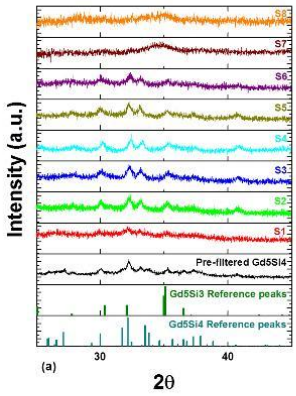

Fractions	Average particles size (nm)	Standard error
S1	688.30	30.71
S2	615.60	35.40
S3	555.54	36.15
S4	468.23	16.80
S5	341.15	8.97
S6	222	7.11
S7	83.84	2.43
S8	82.89	3.81

Standard error of the mean = Standard deviation / √(Sample size)
(b)

FIG. 3. (a) XRD patterns obtained from fractions. Reference peaks of Gd_5Si_4 and Gd_5Si_3 (bottom) matches with the patterns. (b) Average particle sizes decrease across fractions.

fractions are largely amorphous. The deficit of Si in the particle has come from the bulk material. The bulk material was prepared by arc-melting which was reported in the reference number.[4] The deficit in Si in the bulk material could have been a result of incongruent melting of Gd and Si elements in the arc-melter, difference in vapor pressures of the Gd and Si, splintering of individual

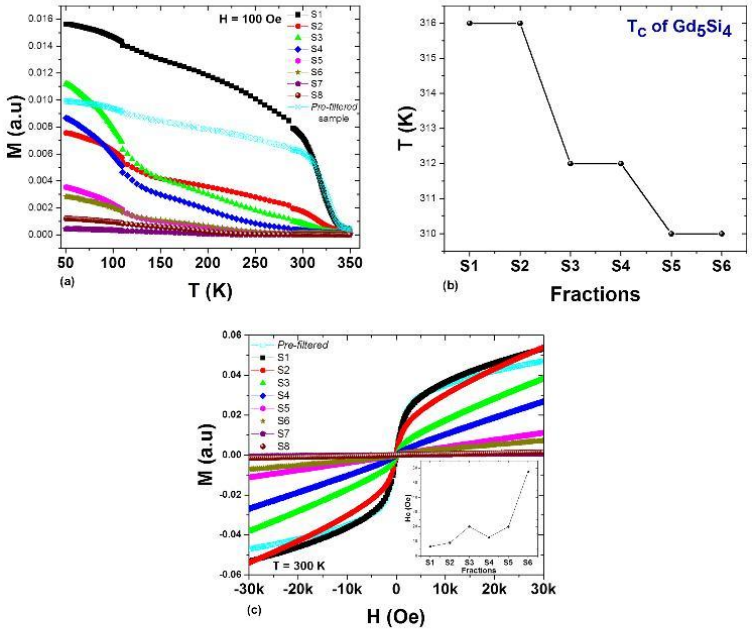

FIG. 4. (a) M-T curve for all fractions and pre-filtered sample (b) Curie temperatures (T_c) for each fraction (*S1-S6*) Gd_5Si_4 powder. (c) M-H curve for all fractions and pre-filtered sample; the figure inset showing coercivity (Hc) with respect to fractions.

elements in the arc-melting process due to uneven heat transfer and low thermal conductivity of Gd and Si.

The VSM measurements show changing Curie temperature for Gd_5Si_4 phase from 316 K for *S1, S2* to 312 K for *S3, S4* to 310 K for *S5, S6* (Fig. 4(b)). Fractions *S7* and *S8* shows no presence of Gd_5Si_4 phase which corroborates with XRD analysis.

The Curie temperatures of all the phases present in the fractions are determined by the intersection point of the steepest tangent (dM/dT) to the M-T curve with the T axis. Curie temperature is observed at 110 K in all separation stages indicating presence of Gd_5Si_3 phase with the volume fraction of this phase increasing in subsequent fractions at the expense of Gd_5Si_4 phase. This is inferred from a qualitative observation made by comparison of the approximate analysis of heights of the M-T curve at the curie temperatures of the respective phases. The increase in Curie temperature of Gd_5Si_3 from 70 K at its bulk form to 110 K in powdered form also reported by Hadimani et al.[4] needs further exploration in order to fundamentally understand the cause for the significant shift in its Curie temperature. Another Curie temperature is observed at 290 K for all fractions indicating the presence of minuscule amount of elemental gadolinium. Presence of elemental gadolinium in the samples may be counter-intuitive as it oxidizes in oxygen rich environments however, the gadolinium oxide forms a barrier shell on the surface preventing further oxidation. Hence, gadolinium can be detected in our M-T measurements. The M-H curves at 300 K exhibits ferromagnetic behavior descending to paramagnetic as we move from *S1* to *S8* fraction. Coercivity (Hc) obtained from hysteresis plots show (inset of Fig. 4(c)) that it increases with decrease in particle size across fractions. This agrees with reports in the literature, where the coercivity increases with decrease in particle size until it reaches single domain and then decreases toward zero where it becomes superparamagnetic.[7,10,17]

CONCLUSION

The study reveals phase and size separation of Gd_5Si_4 nanoparticles could be successfully carried out with the time sensitive sedimentation technique under applied dc magnetic field using a N52 NdFeB permanent magnet. Average nanoparticle sizes decreased as the sedimentation time increased across fractions. Applying dc magnetic field in the separation process resulted in separation of phases (ferromagnetic Gd_5Si_4 phase from paramagnetic Gd_5Si_3 phase and other impurities). Curie temperature of major phase Gd_5Si_4 decreased from 316 K to 310 K across fractions indicating decrease in average Gd_5Si_4 particle sizes while the Curie temperature remained constant at 110 K and 290 K for Gd_5Si_3 phase and elemental gadolinium phase respectively being unaffected by particle size variation.

ACKNOWLEDGMENTS

Synthesis and materials processing at the Ames Laboratory was supported by the Office of Basics Energy Sciences, Materials Science and Engineering Division of the U.S. Department of Energy (DOE). The Ames Laboratory is operated for the U.S. DOE by Iowa State University of Science and Technology under contract No. DE-AC02-07CH11358. Work at VCU was partially funded by National Science Foundation, Award Number: 1610967.

[1] A. A. El-Gendy *et al.*, "Ferromagnetic Gd5Si4 nanoparticles as T2 contrast agents for magnetic resonance imaging," IEEE Magnetics Letters **8**, 1–4 (2017).
[2] R. Richards *et al.*, "High resolution nuclear magnetic resonance," Spectrochimica Acta **16**, 244 (1960).
[3] H. Bin Na, I. C. Song, and T. Hyeon, "Inorganic nanoparticles for MRI contrast agents," Adv. Mater. **21**(21), 2133–2148 (2009).
[4] R. L. Hadimani *et al.*, "Investigation of room temperature ferromagnetic nanoparticles of Gd5Si4," IEEE Trans. Magn. **51**(11), 5–8 (2015).
[5] R. L. Hadimani *et al.*, "First successful fabrication of nanoparticles of magnetocaloric Gd_5Si_4," Bull. Am. Phys. Soc. **60** (2015).
[6] R. Hadimani *et al.*, "Effect of milling time on the blocking temperature of nanoparticles of magnetocaloric Gd_5Si_4," Bull. Am. Phys. Soc. (2016).
[7] S. Chikazumi and C. D. Graham, *Physics of ferromagnetism* (Oxford University Press, 1997).

[8] K. M. Krishnan, "Biomedical nanomagnetics: A spin through possibilities in imaging, diagnostics, and therapy," IEEE Trans. Magn. **46**(7), 2523–2558 (2010).
[9] O. Veiseh *et al.*, "Design and fabrication of magnetic nanoparticles for targeted drug delivery and imaging," Advanced Drug Delivery Reviews **62**(3), 284–304 (2010).
[10] A. Akbarzadeh *et al.*, "Magnetic nanoparticles: Preparation, physical properties, and applications in biomedicine," Nanoscale Res Lett. **7**(1), 144 (2012).
[11] M. Angelakeris, "Magnetic nanoparticles: A multifunctional vehicle for modern theranostics," Biochimica et Biophysica Acta (BBA)–General Subjects **1861**(6), 1642–1651 (2017).
[12] S. Harstad *et al.*, "Enhancement of β-phase in PVDF films embedded with ferromagnetic Gd5Si4 nanoparticles for piezoelectric energy harvesting," AIP Adv. **7**(5) (2017).
[13] H.-J. Weinmann, R. C. Brasch *et al.*, "Characteristics of gadolinium-DTPA complex: A potential NMR contrast agent," AJR Am J Roengenol **142**, 619–624 (1984).
[14] A. Cabrera-García *et al.*, "Gd-Si oxide nanoparticles as contrast agents in magnetic resonance imaging," Nanomaterials **6**(6), 109 (2016).
[15] V. K. Pecharsky *et al.*, J. Alloys Compds. **260**, 98 (1997).
[16] J. Roger, M. B. Yahia *et al.*, J. Solid State Chem. **179**, 2310 (2006).
[17] C. Fermon and M. Van de Voorde, *Nanomagnetism Applications and Perspectives* (Wiley-VCH, 2017).

Conference proceedings

APS March Meeting 2019

View Abstract

CONTROL ID: 3098387

TITLE: A preliminary investigation of large shift in transition temperature (Tc) in Gd_5Si_3 nanoparticles

Abstract Body: Magnetic ordering temperatures in nanostructures depend on size. Curie temperature(Tc) of a bulk material where exchange interactions are comparable to thermal fluctuations tends to decrease in particles. The decrease of ordering temperature with size is described by the scaling theory of Fisher & Barber. However, a large increase in Tc in Gd_5Si_3 NPs have been observed in the ball-milled gadolinium silicide. SEM images shows particle sizes ranging from 50 nm to >2 µm. XRD analysis on pre-separated sample show that ferromagnetic Gd_5Si_4 is the major phase while paramagnetic Gd_5Si_3 is the minor phase. Magnetic properties measured in VSM reveal that the Tc decreases for Gd_5Si_4 phase from 332K for bulk to 315K for ball-milled sample. Another Tc observed at 80K is attributed to Gd_5Si_3 phase undergoes large shift in its transition temperature at 110K and remains constant irrespective of particle sizes.
Plausible reasons for the increase in Tc for Gd_5Si_3 NPs could be due to the effect of high energy mechanical ball-milling process that could induce structural changes, lattice strains, exchange interaction between phases in a particle, or formation of new phase.

Funding Acknowledgement: Work at the Ames Lab was supported by DOE (contract No. DE-AC02-07CH11358). Work at VCU was funded by NSF, Award No.: 1610967.

PRESENTATION TYPE: Poster

UNIT: 10.0 MAGNETISM (GMAG)

SORTING CATEGORY: 10.01.01 Magnetic Nanostructures: Materials and phenomena (GMAG, DMP) [same as 36.10.01.01]

Category Type: Experimental

AUTHORS (FIRST NAME, LAST NAME): Shivakumar Hunagund[1], Shane M. Harstad[1], Shalabh Gupta[2], Vitalij K. Pecharsky[3], Magundappa Hadimani[1]

INSTITUTIONS (ALL): 1. Virginia Commonwealth University, ,
2. Ames Laboratory, US Dept. of Energy, Iowa State University, Ames, IA 50011, null,
3. Dept. of Material Science and Engineering, Ames Laboratory, Iowa State University, Ames, IA 50011, null,

Teams: (none)

Bulletin of the American Physical Society

APS March Meeting 2018
Monday–Friday, March 5–9, 2018; Los Angeles, California

Session G60: Poster Session I
2:00 PM, Tuesday, March 6, 2018
LACC Room: West Hall A

Abstract: G60.00118 : Effect of particle size on Curie temperature and coercivity of Gadolinium silicide (Gd_5Si_4)*

← Abstract →

Presenter:
Shivakumar Hunagund
(Dept. of Mechanical and Nuclear Engineering, Virginia Commonwealth Univ)

Authors:
Shivakumar Hunagund
(Dept. of Mechanical and Nuclear Engineering, Virginia Commonwealth Univ)

Ahmed El-Gendy
(Dept. of Physics, University of Texas at El Paso)

Shalabh Gupta
(Division of Materials Science and Engineering, Ames Laboratory)

Vitalij Pecharsky
(Division of Materials Science and Engineering, Ames Laboratory)

Shane Harstad
(Dept. of Mechanical and Nuclear Engineering, Virginia Commonwealth Univ)

R. L. Hadimani
(Dept. of Mechanical and Nuclear Engineering, Virginia Commonwealth Univ)

Nanoparticles (NP) exhibit different properties from their parent bulk materials due to finite size & surface effects. In this study, size dependent magnetic properties of Gadolinium Silicide (Gd_5Si_4) NP from ball-milled ingot are investigated. NP were size separated into 8 fractions using time sensitive sedimentation in an applied dc magnetic field. SEM image analysis shows average NP sizes of 700nm,615nm,560nm,470nm,342nm,223nm,84nm and 82nm for the 8 corresponding fractions. XRD analysis indicates that Gd_5Si_4 is the major phase and Gd_5Si_3 is the minor phase present in all fractions. VSM measurements reveal that as the NP sizes decreases, the transition temperature (Tc) of Gd_5Si_4 is reduced from 316K to 312K and to 310K, while the ordering of the minor phase is independent of the NP sizes with stagnant Tc at 110K. The M-H curves at 300K exhibits ferromagnetic behavior descending to paramagnetic across fractions. Coercivity (Hc) obtained from hysteresis plots show that Hc increases with decrease in NP size across fractions until it reaches critical single-domain size & then decreases toward zero where it becomes superparamagnetic.

*Work at the Ames Lab was supported by the U.S. DOE(contract No.DE-AC02-07CH11358) and work at VCU was partially funded by NSF, Award No.:1610967.

CONTROL ID: 2943074
PRESENTATION TYPE: Poster
CURRENT CATEGORY: 13. Life sciences applications
CURRENT SUB-CATEGORY: b. Biomedical diagnostics and imaging
TITLE: Effect of Gd_5Si_4 ferromagnetic nanoparticle sizes on T_1, T_2 and T_2^* relaxation in MRI
AUTHORS (LAST NAME, FIRST NAME): Hunagund, Shivakumar[1,2]; Rosenberg, Jens[2]; Harstad, Shane M.[1]; El-Gendy, Ahmed A.[3]; Gupta, Shalabh[4]; Pecharsky, Vitalij[5,4]; Hadimani, Ravi L.[1]
INSTITUTIONS (ALL):
1. Department of Mechanical and Nuclear Engineering, Virginia Commonwealth University, Richmond, VA, United States.
2. The National High Magnetic Field Laboratory, Florida State University, Tallahassee, FL, United States.
3. Dept. of Physics, University of Texas at El Paso, El Paso, TX, United States.
4. Iowa State University, Ames Laboratory, US Department of Energy, Ames, IA, United States.
5. Dept. of Material Science and Engineering, Iowa State University, Ames, IA, United States.
ABSTRACT BODY:
Digest Body: Until now most contrast agents (CA) that are used in Magnetic Resonance Imaging (MRI) studies have been paramagnetic. However, ferromagnetic CAs are potentially more sensitive as T_2 CAs than T_1 paramagnetic compounds due to their large magnetic moments. Previous study has shown that ferromagnetic gadolinium silicide (Gd_5Si_4) nanoparticles (NP) could be useful as potential T_2 CA for MRI with significantly reduced echo time (TE) compared to Superparamagnetic Iron Oxide Nanopartilces (SPION) which are currently the most widely used T_2 CA [1]. Furthermore, the need for better MRI images without the need of upgrading to the higher magnetic field strength can be achieved using better CA such as Gd_5Si_4 NP. The quality of the image contrast in MRI is improved by shortening T_1 and T_2 relaxation times at the site or close proximity to the CA. The efficiency of a T_1 CA is defined by its relaxivity, r_1, which is field and temperature dependent. While, T_2 agents are defined by their relaxivity, r_2, which is dependent on both the saturation magnetization (Ms) value and the effective radius of the NPs [1, 2]. In this study, effect of Gd_5Si_4 NP of varying sizes and with different concentrations are investigated on T_1, T_2 and T_2^* (effective/observed T_2) relaxations times.

Gd_5Si_4 was synthesized by arc-melting of the stoichiometric mixture of gadolinium and silicon under Ar atmosphere and then the Gd_5Si_4 NPs were prepared by high energy ball milling of the crushed ingot. The synthesis process is described in detail elsewhere [3,4]. Ferromagnetic Gd_5Si_4 is extracted with NdFeB grade N52 permanent magnets placed below the beaker containing the ball milled powder in ethyl alcohol before size separating the NPs through time sedimentation process that provided three fractions (named S1, S2 and S3) with average sizes of 586 nm, 287 nm and 135 nm respectively as analyzed from SEM images (Fig. 1). XRD analysis on pre-separated sample show that Gd_5Si_4 is the major phase while GdSi and Gd_5Si_3 is the minor phases present in all fractions (Fig. 1). Magnetic properties measured in VSM reveal that the Curie temperature (Tc) decreases for Gd_5Si_4 phase from 312 K for S1 to 304 K for S2 and is undetectable in S3. Another Tc observed at 105 K can be attributed to Gd_5Si_3 phase. The M-H curves at 300 K exhibits ferromagnetic behavior descending to paramagnetic as we move from S1 to S3 fraction (Fig. 1).

Prior to MRI measurements, NPs are diluted in solution with low-temperature 2% agarose with the following dilutions - 1:20, 1:200, 1:2000 and 1:20000. The high dilution factors were chosen based on solution MRI with lower dilution factors (data not shown) that exhibited extremely strong contrast at 21.1 T and unquantifiable results. Each nanoparticle layer was separated with a 1% agarose layer. MR images were acquired on the 21.1 T (900 MHz) magnet at the National High Magnetic Field Laboratory (NHMFL) in Tallahassee, FL. The magnet is equipped with Bruker Avance III console and Paravision 6.0.1 (Bruker, Ettlingen Germany). For all acquisition a 10-mm birdcage coil was used. Measurements were performed to quantify T_1, T_2 and T_2^* relaxation times for each sample and dilution. For T_1 measurements, a turbo spin echo (TSE) sequence was used with two rare factors. The echo time (TE) was 8.8 ms and ten incrementing (12000 - 26 ms) repetition times (TR) were used. T_2 relaxation were acquired with a multi slice multi echo (MSME) sequence using a TR=5000 ms and 20 incrementing echo time (7.5 – 150 ms). For T_2^*, a 2D gradient echo (GRE) sequence were used with TR=5000ms and eight incrementing TE (1.5 – 28.5 ms). Common acquisition parameters for T_1 and T_2 sequences were 2 averages, matrix = 110x200, FOV = 1.1x 2.0 cm resulting in a 100x100 mm in plane resolution using a 1-mm slice while the 2D T_2^* sequence were acquired with 2 averages and a

matrix of 100x55 resulting in a 200x200 mm in-plane resolution. Magnitude images were analyzed in Paravision using region-of-interest (ROIs) to cover each agarose layer as well as spacing layers. The average signal intensities were extracted and analyzed in Matlab using the Levenberg-Marquardt algorithm. For T_1 a three-parameter exponential growth function were used while for T_2 and T_2^* a three-parameter exponential decay function were employed.
The results shown in Table 1 indicate higher concentrations of NPs shortens the T_2 and T_2^* relaxation times and the contrast disappears rapidly with any higher dilutions. Fraction S2 at 1/20 dilution show notable shortened T_1 and T_2 relaxation times compared to the other two fractions. Although S1 has more Gd_5Si_4 phase volume fraction and larger average particle size compared to S2, further investigation is needed inorder to establish the cause in shortened relaxation times compared to S1 fraction.

Acknowledgements
Synthesis and materials processing at the Ames Lab was supported by DOE (contract No. DE-AC02-07CH11358). Work at VCU was partially funded by NSF, Award Number: 1610967. Part of this work was performed at the NHMFL which is supported by the State of Florida and the NSF cooperative agreement No. DMR-1157490.
References: [1] El-Gendy, A. A. et al. "Ferromagnetic Gd5Si4 Nanoparticles as T2 Contrast Agents for Magnetic Resonance Imaging". IEEE Magnetics Letters 8, 1–4 (2017).
[2] De León-Rodríguez, L. M. et al (2015). "Basic MR relaxation mechanisms and contrast agent design." Journal of Magnetic Resonance Imaging, 42(3), pp.545-565.
[3] Harstad S.M. et al., "Enhancement of β-phase in PVDF films embedded with ferromagnetic Gd5Si4 nanoparticles for piezoelectric energy harvesting," AIP Adv., vol. 7, no. 5, (2017).
[4] Hunagund, S. G., et al. "Investigating phase transition temperatures of size separated gadolinium silicide magnetic nanoparticles". AIP Advances, (In Press).
KEYWORDS: Rare-earth magnetic nanoparticles, MRI contrast agents, Hyperthermia nanoparticles, Magnetocaloric nanoparticles .

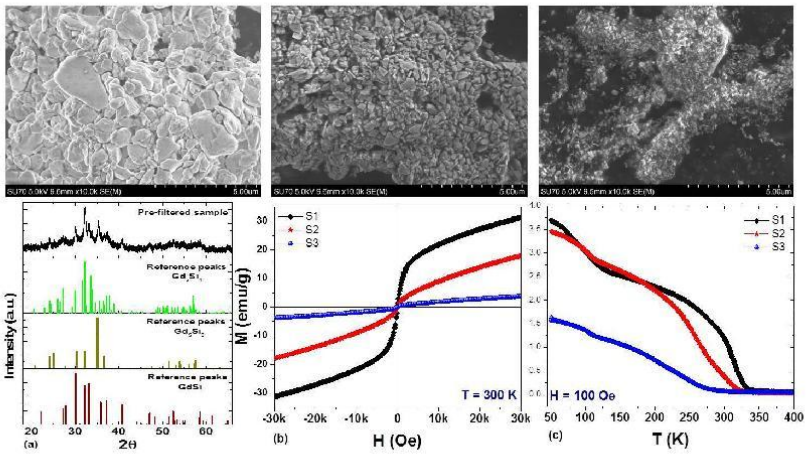

Fig. 1 *(Top row)* SEM images of fractions S1 - S3. *(Bottom row)* (a) XRD patterns obtained from fractions. Reference peaks of Gd_5Si_4, Gd_5Si_3 and GdSi matches with the patterns. (b) M-H curve for all fractions. (c) M-T curve for all fractions.

S1				S2				S3			
Dilution in agarose	T1 (ms)	T2 (ms)	T2* (ms)	Dilution in agarose	T1 (ms)	T2 (ms)	T2* (ms)	Dilution in agarose	T1 (ms)	T2 (ms)	T2* (ms)
1/20	2436.0	38.7	5.2	1/20	1365.9	18.4	1.3	1/20	2438.6	63.4	34.1
1/200	2442.2	59.5	22.7	1/200	1562.5	52.9	24.3	1/200	2681.6	63.4	34.1
1/2000	2706.2	67.5	45.8	1/2000	1673.9	56.3	53.9	1/2000	2785.3	63.2	45.1
1/20000	2768.6	70.2	54.8	1/20000	1777.1	58.6	44.6	1/20000	2726.5	67.9	48.8
1/200000	2685.6	68.0	46.8								
Agarose	2630.2	67.7	46.5	Agarose	1811.4	66.5	54.1	Agarose	2640.0	75.8	51.8

Table. 1 - T_1, T_2 and T_2^* relaxation times of S1, S2 and S3 fractions at different concentrations.

IMAGE CAPTION: Fig. 1 *(Top row)* SEM images of fractions S1 - S3. *(Bottom row)* (a) XRD patterns obtained from fractions. Reference peaks of Gd_5Si_4, Gd_5Si_3 and GdSi matches with the patterns. (b) M-H curve for all fractions. (c) M-T curve for all fractions. Table. 1 - T_1, T_2 and T_2^* relaxation times of S1, S2 and S3 fractions at different concentrations.

CONTACT (NAME ONLY): Shivakumar Hunagund
CONTACT (EMAIL ONLY): hunagunds@vcu.edu

AWARDS:

Previous Presentation: Yes

Manuscript?: Undecided

Attendance at Conference: I acknowledge that I have read the above statement regarding the requirement that an author of this presentation must attend the conference to present the paper.